Inorganic Chemistry

Article

pubs.acs.org/IC

The Series of Molecular Conductors and Superconductors $ET_4[AFe(C_2O_4)_3]\cdot PhX$ (ET = bis(ethylenedithio)tetrathiafulvalene; $(C_2O_4)^{2-}$ = oxalate; $A^+ = H_3O^+, K^+$; X = F, Cl, Br, and I): Influence of the Halobenzene Guest Molecules on the Crystal Structure and Superconducting Properties

Eugenio Coronado, Simona Curreli, Carlos Giménez-Saiz,* and Carlos J. Gómez-García*

Instituto de Ciencia Molecular (ICMol), Parque Científico, Universidad de Valencia, 46980 Paterna, Valencia, Spain

Supporting Information

ABSTRACT: An extensive series of radical salts formed by the organic donor bis(ethylenedithio)tetrathiafulvalene (ET), the paramagnetic tris(oxalato)-ferrate(III) anion $[Fe(C_2O_4)_3]^{3-}$, and halobenzene guest molecules has been synthesized and characterized. The change of the halogen atom in this series has allowed the study of the effect of the size and charge polarization on the crystal structures and physical properties while keeping the geometry of the guest molecule. The general formula of the salts is $ET_4[A^IFe(C_2O_4)_3]\cdot G$ with A/G = H_3O^+/PhF (**1**); H_3O^+/PhCl (**2**); H_3O^+/PhBr (**3**), and K^+/PhI (**4**), (crystal data at room temperature: (**1**) monoclinic, space group $C2/c$ with a = 10.3123(2) Å, b = 20.0205(3) Å, c = 35.2732(4) Å, β = 92.511(2)°, V = 7275.4(2) Å^3, Z = 4; (**2**) monoclinic, space group $C2/c$ with a = 10.2899(4) Å, b = 20.026(10) Å, c = 35.411(10) Å, β = 92.974°, V = 7287(4) Å^3, Z = 4; (**3**) monoclinic, space group $C2/c$ with a = 10.2875(3) Å, b = 20.0546(15) Å, c = 35.513(2) Å, β = 93.238(5)°, V = 7315.0(7) Å^3, Z = 4; (**4**) monoclinic, space group $C2/c$ with a = 10.2260(2) Å, b = 19.9234(2) Å, c = 35.9064(6) Å, β = 93.3664(6)°, V = 7302.83(18) Å^3, Z = 4). The crystal structures at 120 K evidence that compounds **1**−**3** undergo a structural transition to a lower symmetry phase when the temperature is lowered (crystal data at 120 K: (**1**) triclinic, space group $P\bar{1}$ with a = 10.2595(3) Å, b = 11.1403(3) Å, c = 34.9516(9) Å, α = 89.149(2)°, β = 86.762(2)°, γ = 62.578(3)°, V = 3539.96(19) Å^3, Z = 2; (**2**) triclinic, space group $P\bar{1}$ with a = 10.25276(14) Å, b = 11.15081(13) Å, c = 35.1363(5) Å, α = 89.0829(10)°, β = 86.5203(11)°, γ = 62.6678(13)°, V = 3561.65(8) Å^3, Z = 2; (**3**) triclinic, space group $P\bar{1}$ with a = 10.25554(17) Å, b = 11.16966(18) Å, c = 35.1997(5) Å, α = 62.7251(16)°, β = 86.3083(12)°, γ = 62.7251(16)°, V = 3575.99(10) Å^3, Z = 2; (**4**) monoclinic, space group $C2/c$ with a = 10.1637(3) Å, b = 19.7251(6) Å, c = 35.6405(11) Å, β = 93.895(3)°, V = 7128.7(4) Å^3, Z = 4). A detailed crystallographic study shows a change in the symmetry of the crystal for compound **3** at about 200 K. This structural transition arises from the partial ordering of some ethylene groups in the ET molecules and involves a slight movement of the halobenzene guest molecules (which occupy hexagonal cavities in the anionic layers) toward one of the adjacent organic layers, giving rise to two nonequivalent organic layers at 120 K (compared to only one at room temperature). The structural transition at about 200 K is also observed in the electrical properties of **1**−**3** and in the magnetic properties of **1**. The direct current (dc) conductivity shows metallic behavior in salts **1**−**3** with superconducting transitions at about 4.0 and 1.0 K in salts **3** and **1**, respectively. Salt **4** shows a semiconductor behavior in the temperature range 300−50 K with an activation energy of 64 meV. The magnetic measurements confirm the presence of high spin S = 5/2 $[Fe(C_2O_4)_3]^{3-}$ isolated monomers together with a Pauli paramagnetism, typical of metals, in compounds **1**−**3**. The magnetic properties can be very well reproduced in the whole temperature range with a simple model of isolated S = 5/2 ions with a zero field splitting plus a temperature independent paramagnetism (Nα) with the following parameters: g = 1.965, $|D|$ = 0.31 cm^{-1}, and Nα = 1.5 × 10^{-3} emu mol^{-1} for **1**, g = 2.024, $|D|$ = 0.65 cm^{-1}, and Nα = 1.4 × 10^{-3} emu mol^{-1} for **2**, and g = 2.001, $|D|$ = 0.52 cm^{-1}, and Nα = 1.5 × 10^{-3} emu mol^{-1} for **3**.

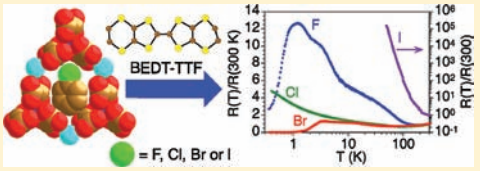

INTRODUCTION

Currently, one of the most appealing aims in the field of (multi)functional materials is the synthesis of hybrids that combine conductivity with magnetism in the same crystal lattice.[1−5] This novel class of materials should provide a unique opportunity to study the physics arising from the competition and interplay of these two properties. So far, a rich harvest of hybrid materials combining magnetism with conductivity has been produced, including examples of paramagnetic[1,6−10] or antiferromagnetic[11−16] superconductors and ferromagnetic conductors.[4,17] Many of these promising results have been obtained using tris(oxalato)metalate complexes, $[M(C_2O_4)_3]^{n-}$, as magnetic counter-anions in the preparation of conducting radical cation salts with donors of the tetrathiafulvalene (TTF) family. In these radical salts the oxalato complexes may crystallize as isolated anions, oligomers, and, finally, as extended layers.

Received: October 19, 2011
Published: December 23, 2011

   dx.doi.org/10.1021/ic202269x | *Inorg. Chem.* 2012, 51, 1111−1126

Isolated anions have been observed in radical salts with different donors. Thus, with TTF there are two known salts with 7:2 and 3:1 stoichiometries: $(TTF)_7[Fe(C_2O_4)_3]_2{\cdot}4H_2O$[18] and $(TTF)_3[Ru(C_2O_4)_3]{\cdot}(EtOH)_{0.5}{\cdot}4H_2O$.[19] With bis(ethylenediseleno)-tetrathiafulvalene (BEST) there are five known salts, four with 4:1 stoichiometry: $(BEST)_4[M(C_2O_4)_3]{\cdot}PhCOOH{\cdot}H_2O$ (M = Cr and Fe)[20] and $(BEST)_4[M(C_2O_4)_3]{\cdot}1.5H_2O$ (M = Cr and Fe),[20] and one with 9:2 stoichiometry: $(BEST)_9[Fe(C_2O_4)_3]_2{\cdot}7H_2O$.[20] Finally, with bis(ethylenedithio)-tetrathiafulvalene (ET) there are at least seven salts with different stoichiometries including two examples containing also Na^+ cations besides the ET molecules: $(ET)_{12}[Fe(C_2O_4)_3]_2{\cdot}nH_2O$,[21] $(ET)_2[Ge(C_2O_4)_3]{\cdot}PhCN$,[22] $(ET)_9Na_{18}[M(C_2O_4)_3]_8{\cdot}24H_2O$ (M^{III} = Fe and Cr)[23,24] $(ET)_5[Fe(C_2O_4)_3]{\cdot}CH_2Cl_2{\cdot}2H_2O$,[25] $(ET)_5[Ge(C_2O_4)_3]_2$[26] and $(ET)_7[Ge(C_2O_4)_3](CH_2Cl_2)_{0.87}(H_2O)_{0.09}$.[26]

Besides isolated monomers, tris(oxalato)metalate complexes also crystallize forming previously unknown $[M_2(C_2O_4)_5]^{4-}$ dimers (M^{III} = Fe and Cr) with TTF, TMTTF and ET[18,27] or even $[\{M^{III}(C_2O_4)_3\}_2M^{II}(H_2O)_2]^{4-}$ trimers (M^{III} = Cr and Fe; M^{II} = Mn, Fe, Co, Ni, Cu, and Zn), prepared with TTF.[28,29]

Nevertheless, the most common packing observed for radical salts of ET with tris(oxalato)metalate complexes is the one in honeycomb-like two-dimensional (2D) anionic layers. This packing, formed with the help of a divalent M^{II} cation, has been observed in the molecular ferromagnetic metals: $(ET)_x[M^{II}M^{III}(C_2O_4)_3]$ ($M^{II}M^{III}$ = MnCr, CoCr and MnRh, $x \approx 2.5-3.0$) and $(BETS)_x[MnCr(C_2O_4)_3]{\cdot}CH_2Cl_2$ (BETS = bis(ethylenedithio)tetraselenafulvalene; $x \approx 3$).[4,17,30−36] Interestingly, similar honeycomb 2D layers can also be obtained with the help of monovalent cations (A^+), although in this case the magnetic coupling is canceled since these cations are diamagnetic. Nevertheless, this strategy has given rise to the largest known series of paramagnetic superconductors, metals, and semiconductors (Tables 1 and 2). This series can be formulated as $(ET)_4[A^IM^{III}(C_2O_4)_3]{\cdot}G$ ($A^I = H_3O^+$, NH_4^+, and K^+; M^{III} = Fe, Cr, Ga, Co, Mn, and Al; G = $PhNO_2$, PhCN, py, $PhCl_2$, PhBr, $PhCOCH_3$, $PhCH_2OHCH_3$, Me_2NCHO, CH_2Cl_2, $PhN(CH_3)CHO$, $PhCH_2CN$,···) and presents up to four different polymorphs: (1) a monoclinic ($C2/c$) β'' phase, (2) an orthorhombic ($Pbcn$) *pseudo*-κ phase, (3) a triclinic (P1) $\alpha\beta''$, and (4) a triclinic ($P\bar{1}$) α-pseudo-κ phase (Tables 1 and 2). The main difference[37,38] between these four polymorphs resides in the packing of the organic layers: (1) parallel ET molecules in the monoclinic β'' phase, (2) ET dimers surrounded by monomers in the orthorhombic pseudo-κ phase, (3) a mixture of α and β'' layers in the $\alpha\beta''$ phase and (4) a mixture of α and pseudo-κ layers in the α-pseudo-κ phase. As expected, these structural differences also lead to different physical properties. Thus, the orthorhombic and triclinic salts are semiconductors whereas the monoclinic salts are metallic and, in some cases, superconductors (Tables 1 and 2).

The monoclinic series represents a good example of the possibilities offered by the molecular approach to tune the properties of the material. Thus, by simply changing the organic guest molecule (G) that sits in a pseudohexagonal cavity created by the anionic magnetic sublattice, it is possible to induce drastic differences in the transport properties. From its position in this cavity the guest molecule is able to affect the conformation and structural order/disorder of the ethylene groups of the nearest donor molecules, a fact that could determine the (de)stabilization of the superconducting state.[57] The crystal structures reveal that more ordered ethylene groups are found when G contains a phenyl ring linked to a small substituent (such as -CN or $-NO_2$).[7,8,43,56,58] Thus, the radical salts containing PhCN or $PhNO_2$ are superconductors and have

Table 1. Structural and Electrical Properties of the Fe-Containing $ET_4[A^IFe^{III}(C_2O_4)_3]{\cdot}G$ Salts

	A^I	G	ET packing	space group	electrical properties	ref	CCDC code
a	H_3O^+	PhCN	β''	$C2/c$	T_c = 7.0−8.5 K	7,8,39−41	ZYGYET
	H_3O^+	C_5H_5N	β''	$C2/c$	T_{MI} = 116 K	40,42	BEMPEO
a	H_3O^+/ NH_4^+	$PhNO_2$	β''	$C2/c$	T_c = 6.2 K	43	ECOPIV
	H_3O^+	$PhNO_2$	β''	$C2/c$	semicond	44,45	COQNEB
	H_3O^+	$PhCl_2$	β''	$C2/c$	T_{MI} = 3.0 K	41,46	PONMEL
					metal >1.5 K		
	H_3O^+	$PhBr_2$	α-pseudo-κ	$P\bar{1}$	metal >1.5 K	41,47	
a	H_3O^+	PhBr	β''	$C2/c$	T_c = 4.0 K	48	SAPWEM
	NH_4^+	DMF	β''	$C2/c$	metal >4 K	49	UMACEQ
a	H_3O^+	PhF	β''	$C2/c$	T_c = 1.0 K	41	UJOXEX
						this work	749412, 837031
a	H_3O^+	PhCl	β''	$C2/c$	metal	41,50,51	UJOXAT
						this work	240173, 837032
a	H_3O^+	PhF/PhCN	β''	$C2/c$	T_c = 6.0 K	41	UJOXIB
a	H_3O^+	$PhCl_2$/PhCN	β''	$C2/c$	T_c = 7.2 K	41	UJOXOH
	H_3O^+	PhF/PhCN	pseudo-κ	$Pbcn$	semiconductor	41	UJOXUN
a	H_3O^+	PhCl/PhCN	β''	$C2/c$	T_c = 6.0 K, superconducting	41	UJOYAU
a	H_3O^+	PhBr/PhCN	β''	$C2/c$	T_c = 4.2 K	41	UJOYEY
	K^+	PhI	β''	$C2/c$	E_a = 64 meV	this work	837030, 837034
	NH_4^+	PhCN	pseudo-κ	$Pbcn$	E_a = 140 meV	8,39	ZIWNEY
	K^+	PhCN	pseudo-κ	$Pbcn$	E_a = 141 meV	8	ZIWNIC
	NH_4^+	$PhCOCH_3$	$\alpha\beta''$	$P\bar{1}$	no supercond	52	ARABEA
	NH_4^+	*R*/*S*-$PhCH_2OHCH_3$	$\alpha\beta''$	$P\bar{1}$	T_{MI} = 170 K	53	CILDIL
	NH_4^+	*S*-$PhCH_2OHCH_3$	$\alpha\beta''$	P1	T_{MI} = 150 K	53	NIPTEM
	K^+	PhCl	β''		semicond.	54	
	Rb^+	C_5H_5N	β''		metal >4.2 K	50	

[a]Superconducting salt.

dx.doi.org/10.1021/ic202269x | *Inorg. Chem.* 2012, 51, 1111−1126

Table 2. Structural and Electrical Properties of the $ET_4[A^IM^{III}(C_2O_4)_3]\cdot G$ Salts with $M \neq Fe^{III}$

	M^{III}	A^I	G	ET packing	space group	electrical properties	ref	CCDC code
a	Cr	H_3O^+	PhCN	β''	$C2/c$	T_c = 5.5−6.0 K	37,39	JUPGUW01
	Cr	H_3O^+	CH_2Cl_2	β''	$C2/c$	T_{MI} = 150 K	55	MEQZIR
a	Cr	H_3O^+/NH_4^+	$PhNO_2$	β''	$C2/c$	T_c = 5.8 K	43	ECOPUH
a	Cr	H_3O^+	PhBr	β''	$C2/c$	T_c = 1.5 K	51	240302
	Cr	H_3O^+	PhCl	β''	$C2/c$	T_{MI} = 130 K	51	240172
	Cr	K^+/NH_4^+	DMF	β''	$C2/c$	metal >4 K	49	UMACAM
	Cr	K^+	DMF	β''	$C2/c$	metal >4 K	49	UMACIU
	Cr	H_3O^+	PhCN	pseudo-κ	*Pbcn*	E_a = 153 meV	37,39	JUPGUW
a	Ga	H_3O^+	C_5H_5N	β''	$C2/c$	$T_c \approx 2$ K	56	HUNQIQ
a	Ga	H_3O^+	$PhNO_2$	β''	$C2/c$	T_c = 7.5 K	56	HUNQUC
	Ga	NH_4^+	PhN(Me)CHO	$\alpha\beta''$	$P\bar{1}$	semicond	52	AQUZUH
	Ga	NH_4^+	$PhCH_2CN$	$\alpha\beta''$	$P\bar{1}$	semicond	52	ARABAW
a	Mn	H_3O^+	PhBr	β''	$C2/c$	T_c = 2.0 K	*b*	
	Co	NH_4^+	PhCN	pseudo-κ	*Pbcn*	E_a = 225 meV	39	QIWMOY
	Al	NH_4^+	PhCN	pseudo-κ	*Pbcn*	E_a = 222 meV	39	QIWMUE

[a]Superconducting salt. [b]C. J. Gómez-García et al. manuscript in preparation.

the highest T_c's in these series: 5.8, 6.2, and 7.5 K for G = $PhNO_2$ and M = Cr, Fe and Ga, respectively, or 6.0 and 8.5 K for G = PhCN and M = Cr and Fe (Tables 1 and 2). In contrast, for G = pyridine, a disorder, which persists at low temperatures, is found in the ethylene groups, and the salts either do not exhibit a superconducting transition (M = Fe),[42] or it appears at temperatures below 2 K (M = Ga).[56] A similar structural disorder has been found in salts containing dichloromethane[55] or dimethylformamide[49] as guests, which do not show superconductivity. Furthermore, two recent studies performed with mixtures of PhCN and other solvents as C_5H_5N, $PhCl_2$, $PhNO_2$, PhF, PhCl, or PhBr as guest molecules show that the presence of the superconducting transition and its critical temperature can be modulated by changing the composition of the mixture.[40,41]

When other benzene-type solvents containing more bulky substituents are used, the resulting structures are triclinic and show double organic layers with α and β'' packing (Tables 1 and 2). These triclinic salts are all semiconductors or present metal−insulator transitions at low temperatures.[52,53] A different semiconducting triclinic phase has been very recently obtained using the chiral solvent (*R*)-(-)-carvone.[24,59] In contrast to other examples with chiral anions as $[M(C_2O_4)_3]^{3-}$, $[Cr(2,2'\text{-bipy})(C_2O_4)_2]^-$,[60] $[Fe(C_5O_5)_3]^{3-}$[62] and trisphat,[63] this strategy has led to two of the very few examples[64,65] of chiral conducting salts: $(ET)_3[NaCr(C_2O_4)_3]\cdot G$ (G = CH_2Cl_2 and CH_3NO_2). The chirality in these salts comes from the fact that there is an excess of one of the enantiomers (64:36 if G = CH_3NO_2 and 56:44 if G = CH_2Cl_2). Nevertheless, the stoichiometry is different (3:1) as a consequence of the smaller size of the hexagonal cavities, and these salts are semiconductors with E_a in the range 69−80 meV.[24,59]

All these data show the important role of the G molecule in determining the structure and physical properties of these radical salts. Although the number of used guest molecules is quite high (see Tables 1 and 2), their geometries are different (except for PhCl and PhBr) and, therefore, besides the effect of the size, there is also an additional effect of the geometry. To remove the geometry effects and, therefore, to study exclusively the effect of the size of G, we have used four monohalobenzene guest molecules (PhX, X = F, Cl, Br, and I) to prepare the series of radical salts $\beta''\text{-}(ET)_4[AFe(C_2O_4)_3]\cdot G$ where A/G = H_3O^+/PhF (**1**), H_3O^+/PhCl (**2**), H_3O^+/PhBr (**3**), and K^+/PhI (**4**). In this work we will show that this series offers a unique opportunity to check the role played by the polarizing effect of the halogen atom of the guest molecule on the order/disorder and conformation of the ethylene groups of the ET molecules, and therefore in the occurrence of the superconducting transition.[57,66]

Preliminary accounts on salts containing PhBr[48,67] and PhCl[50,51] as guest molecules have already been published by us and others. In these two examples, a static disorder in the ethylene groups of the donors was observed at room temperature. However, the bromobenzene derivative exhibits superconductivity at T_c = 4.0 K,[48,67] suggesting that an ordering of the ethylene groups could take place at low temperatures. In fact, preliminary X-ray studies indicated that the PhBr derivative exhibits a structural phase transition in the temperature range 180−160 K.[48] In contrast, in the chlorobenzene derivative no superconducting transition has been observed down to 0.4 K. Finally, in 2007 we presented a preliminary report of the superconducting PhF derivative (T_c = 1.0 K)[68] and, very recently, other researchers also reported the synthesis of this salt, although they did not find any superconducting transition above 1.5 K.[41]

EXPERIMENTAL SECTION

Synthesis. The organic donor ET, the 18-crown-6 ether, and all the solvents used in this work were purchased from Fluka and used as received. The potassium salt $K_3[Fe(C_2O_4)_3]\cdot 3H_2O$, was prepared as previously reported[69] and recrystallized several times from water. The radical salts were prepared by electrochemical oxidation of the donor on platinum wire electrodes in U-shaped cells under low constant current. The anodic and cathodic compartments are separated by a porous glass frit. The exact conditions for the synthesis of each particular radical salt are described below.

Synthesis of $ET_4[(H_3O)Fe(C_2O_4)_3]\cdot G$, G = PhF (1), PhCl (2), or PhBr (3). A solution of racemic $K_3[Fe(C_2O_4)_3]\cdot 3H_2O$ (56.5 mg, 5 mM) and 18-crown-6 ether (91.2 mg, 1.5×10^{-2} M) in a mixture of 3 mL of MeOH and 20 mL of fluorobenzene (for **1**), chlorobenzene (for **2**), or bromobenzene (for **3**) was distributed between the two compartments of a U-shaped cell. Solid ET (8 mg) was introduced in the anode compartment, and a constant current of 1 μA was applied. Prismatic crystals with nearly square cross section were collected from the anode after 7−10 days.

Synthesis of $ET_4[KFe(C_2O_4)_3]\cdot PhI$, (4). A solution of racemic $K_3[Fe(C_2O_4)_3]\cdot 3H_2O$ (56.5 mg, 5 mM), 18-crown-6 ether (91.2 mg, 1.5×10^{-2} M) and 4-cyanopyridine (479 mg, 0.2 M) in a mixture of 3 mL of acetonitrile and 20 mL of iodobenzene was distributed between the two compartments of a U-shaped cell. Solid ET (8 mg) was introduced in the anode compartment, and a constant current of

dx.doi.org/10.1021/ic202269x | Inorg. Chem. 2012, 51, 1111−1126

1 μA was applied. Prismatic crystals of **4** with nearly square cross section were collected from the anode after 18 days.

Structure Determination. X-ray diffraction data of compounds **1**−**3** at room temperature were collected with a Nonius KappaCCD diffractometer using a graphite monochromated Mo−Kα radiation source (λ = 0.71073 Å). Denzo and Scalepack[70] programs were used for cell refinements and data reduction. Multiscan absorption corrections, based on equivalent reflections, were applied to the data using the program SORTAV.[71] For compounds **1**−**3** at 120(2) K and compound **4** at 292(2) and 120(2) K X-ray diffraction data were collected with an Oxford Diffraction Xcalibur diffractometer equipped with a Sapphire 3 CCD detector. The data collection routines, unit cell refinements, and data processing were carried out with the program CRYSALIS.[72] Analytical numeric absorption corrections were applied to the data using the multifaceted crystal model[73] integrated in the program CRYSALIS. All structures were solved by direct methods using the SIR97[74] program with the WinGX[75] graphical interface. The structure refinements were carried out with SHELX-97.[76] All non-hydrogen atoms were refined anisotropically. For structures of **1**−**3** at 120(2) K some restraints (DELU, SIMU) were applied on the anisotropic displacement parameters of disordered ethylene groups to prevent them to go "non-positive definite". Hydrogen atoms on carbon atoms were included at calculated positions and refined with a riding model. Hydrogen atoms of hydronium ions were not located. Crystal data are tabulated in Table 3.

Compounds **1**−**4** were found to be isostructural at room temperature, exhibiting good diffraction patterns corresponding to monoclinic unit cells (Table 3) typical of the other members of this series of compounds. However, as the temperature is lowered, the diffraction patterns of compounds **1**−**3** start exhibiting some problems: an increase of the mosaicity, a significant overlap of some reflection profiles and a decrease in the number of indexed reflections (only 50−70% of the reflections were indexed, depending on the particular crystal tested). The overlap of reflections persisted even when the crystals were reoriented to align the longest axis (*c*) close to the spindle axis of crystal rotation or when the crystal-to-detector distance was increased from 50 to 80 mm. Moreover, as the temperature is lowered, the unit cell parameters of **1**−**3** gradually vary in such a way that below a certain temperature their unit cells cannot longer be considered as monoclinic and are better described by their triclinic reduced (or Niggli) cells. All these data point to a structural phase transition with a change in the symmetry of the crystals from monoclinic to triclinic in compounds **1**−**3**. This transition can be monitored with the variation of the corresponding α (or γ) parameters of the unit cell that start to deviate from 90° at the temperature at which the transition can be considered to take place (i.e., below ∼200 K for compound **3**, see below). It is worth noting that the mentioned problems in the diffraction patterns disappear when the temperature is raised again to room temperature, when almost 100% of the reflections can be indexed again in the original monoclinic unit cell. This reversible behavior might be because the structural transition observed when lowering the temperature is neither complete nor homogeneous, probably because of low kinetics of the transformation in the tested temperature range (from 300 to ∼100 K). This incomplete structural phase transition would cause the previously mentioned reflections overlap, as well as a significant dispersion of the diffraction spots around the reciprocal lattice points. This dispersion is evident when the reciprocal space is looked at down the *a** or *b** directions, therefore revealing a change in the value and direction of the *c* axis (the longest axis of the crystal). The crystallographic *c* direction is perpendicular to the layers that build up the crystal structure (see structural description). A change in the value of this axis could be due to a progressive and nonregular (in the bulk of the crystal) ordering/disordering process of the ethylene groups of the ET molecules when the temperature is lowered (the ethylene groups are the interacting part of the ET sublattice with the anionic one). An ordering of the ethylene groups at low temperatures also takes place in the radical salt β-ET_2I_3 (a long-range ordering in this case) resulting in an incommensurate modulated phase transition with origin in H···I type crystal packing interactions between the ET molecules and the tri-iodide anions.[77] For compounds **1**−**3**, however, all attempts to treat the data as a modulated structure or a twining were not satisfactory (X-ray data were collected on several crystals of each compound giving similar results in all cases). Therefore, the crystal structures presented for **1**−**3** at 120 K must be considered as "average" structures, exhibiting high R factors because of the problems previously described. In contrast, compound **4** exhibits the same monoclinic unit cell at room temperature and at 120 K, with no signs of any structural transition in that temperature range.

Conductivity Measurements. Direct current (dc) conductivity measurements over the temperature range 0.4−300 K were performed with the four contacts method for several single crystals of each salt, giving reproducible results in all the samples. In compound **4** the resistance of the samples below about 50 K was too high (>20 MΩ) to

Table 3. X-ray Crystallographic Data for $ET_4[A^IFe(C_2O_4)_3]\cdot G$ with A^I/G = H_3O/PhF (1), H_3O/PhCl (2), H_3O/PhBr (3) and K/PhI (4)

	1		2		3		4	
A^I/G	H_3O/PhF		H_3O/PhCl		H_3O/PhBr		K/PhI	
chem formula	$C_{52}H_{40}FFeO_{13}S_{32}$		$C_{52}H_{40}ClFeO_{13}S_{32}$		$C_{52}H_{40}BrFeO_{13}S_{32}$		$C_{52}H_{37}IFeKO_{12}S_{32}$	
fw	1973.61		1990.06		2034.52		2101.59	
T/K	**292(2)**	**120(2)**	**293(2)**	**120(2)**	**292(2)**	**120(2)**	**292(2)**	**120(2)**
a (Å)	10.3123(2)	10.2595(3)	10.2899(4)	10.25276(14)	10.2875(3)	10.25554(17)	10.2260(2)	10.1637(3)
b (Å)	20.0205(3)	11.1403(3)	20.026(10)	11.15081(13)	20.0546(15)	11.16966(18)	19.9234(2)	19.7251(6)
c (Å)	35.2732(4)	34.9516(9)	35.411(10)	35.1363(5)	35.513(2)	35.1997(5)	35.9064(4)	35.6405(11)
α (deg)	90	89.149(2)	90	89.0829(10)	90	89.1001(12)	90	90
β (deg)	92.511(2)	86.762(2)	92.974(5)	86.5203(11)	93.238(5)	86.3083(12)	93.3664(6)	93.895(3)
γ (deg)	90	62.578(3)	90	62.6678(13)	90	62.7251(16)	90	90
V (Å^3)	7275.4(2)	3539.96(19)	7287(4)	3561.65(8)	7315.0(7)	3575.99(10)	7302.83(18)	7128.7(4)
Z^a	4	2	4	2	4	2	4	4
cryst syst	monoclinic	triclinic	monoclinic	triclinic	monoclinic	triclinic	monoclinic	monoclinic
space group	*C*2/*c*	$P\bar{1}$	*C*2/*c*	$P\bar{1}$	*C*2/*c*	$P\bar{1}$	*C*2/*c*	*C*2/*c*
ρ_{calcd}/g cm^{-3}	1.802	1.852	1.814	1.856	1.847	1.889	1.911	1.958
GOF	1.065	1.156	1.056	1.206	1.060	1.155	1.024	1.021
μ/mm^{-1}	1.188	1.221	1.221	1.249	1.726	1.765	1.660	1.700
$R(F_o)$	0.0396	0.1815	0.0623	0.1369	0.0487	0.1884	0.0486	0.0330
$R_w(F_o^2)$ $[I < 2\sigma(I)]^b$	0.1117	0.3770	0.1218	0.3116	0.1089	0.4307	0.1212	0.0782

^aZ = number of chemical formula per unit cell. $^bR = \sum||F_o| - |F_c||/\sum|F_o|$. $R_w = \{\sum w(F_o^2 - F_c^2)^2/\sum w(F_o^2)^2\}^{1/2}$.

dx.doi.org/10.1021/ic202269x | *Inorg. Chem.* 2012, 51, 1111−1126

be measured with our equipment. The contacts between the platinum wires (25 μm diameter) and the samples were done using graphite paste. All the samples were measured with cooling and warming rates of 1 K min^{-1} giving similar results within experimental error and with dc intensity currents in the range 0.1−50 μA, also with similar results, in a Quantum Design PPMS-9. The magneto-resistance measurements were performed with magnetic fields of up to 9 T applied parallel to the conducting layers.

Magnetic Measurements. Variable temperature susceptibility measurements were carried out in the temperature range 2−300 K with an applied magnetic field of 0.1 T on polycrystalline samples of **1**−**3** with a Quantum Design MPMS-XL-5 SQUID magnetometer. The susceptibility data were corrected for the sample holder previously measured using the same conditions and for the diamagnetic contributions of the salt as deduced by using Pascal constant tables ($\chi_{dia} = -1006.53 \times 10^{-6}$, -1020.33×10^{-6}, and -1030.83×10^{-6} emu mol^{-1} for **1**−**3**, respectively).[78] The synthesis of sample **4** yielded only a few crystals that were used for the X-ray structure determination and for the conductivity measurements, precluding the performance of reliable magnetic measurements.

RESULTS AND DISCUSSION

Synthesis. A rational method to obtain new conductors and superconductors of general formula $ET_4[AFe(C_2O_4)_3]\cdot G$ consists of using as solvent in the electrocrystallization synthesis the guest molecule we want to insert in the pseudohexagonal cavity created by the inorganic sublattice (G). Using this simple approach, compounds **1** (G = PhF), **2** (G = PhCl), and **3** (G = PhBr) are easily obtained. In all cases methanol is added to increase the solubility of the inorganic salt in the organic solvent, but its use is not compulsory. However, when PhI is used as solvent, no crystals are formed on the electrode. This result suggests that the use of PhI as solvent could be a good strategy to insert other guest molecules, including those that are solids at room temperature and therefore cannot be used as solvents themselves in the electrocrystallization experiments. Surprisingly, the use of 4-cyanopyridine dissolved in PhI (together with some acetonitrile to increase the solubility of the inorganic salt) in the electrocrystallization process produces crystals of compound **4** in which G is PhI instead of 4-cyanopyridine. Moreover, as a distinctive characteristic of **4**, the monocation A^+ is found to be K^+ instead of hydronium (H_3O^+) as in **1**−**3**. In these salts potassium can be clearly distinguished from oxygen by X-ray single-crystal diffraction, and its presence was also confirmed by microanalysis. Therefore, these results illustrate the difficulty in rationalizing the electrocrystallization technique when applied to the synthesis of molecular conductors, which is frequently based on the trial and error method.

Crystal Structures of $ET_4[AFe(C_2O_4)_3]\cdot G$ [A/G = H_3O^+/PhF (1), H_3O^+/PhCl (2), H_3O^+/PhBr (3), and K^+/PhI (4)] at Room Temperature. The X-ray analysis at room temperature shows that compounds **1**−**4** are isostructural to the aforementioned monoclinic series β''-$ET_4[AM(C_2O_4)_3]\cdot G$ (M = Fe, Cr, Ga,···; A = H_3O^+, NH_4^+, K^+,···; and G = PhCN, $PhNO_2$, DMF, CH_2Cl_2,···; see Tables 1 and 2). However, compounds **1**−**4** provide a unique opportunity to study the subtle structural changes caused in the ET and oxalato sublattices of these radical salts as the halogen atom of the guest molecule (G) is changed from F to I. First, however, the general features for all four compounds will be outlined.

Compounds **1**−**4** crystallize in the monoclinic space group $C2/c$ (Table 3). The asymmetric units contain two independent ET molecules (labeled as A and B) lying on general positions, half tris(oxalato)ferrate anion, half halobenzene molecule, and half hydronium cation (for **1**−**3**) or half potassium cation (for **4**), all lying on a 2-fold rotation axis. Figure 1 shows a standard ellipsoid diagram of the molecules in **2** together with the atom-labeling scheme of all four compounds (of course, the only difference corresponds to the halogen atom).

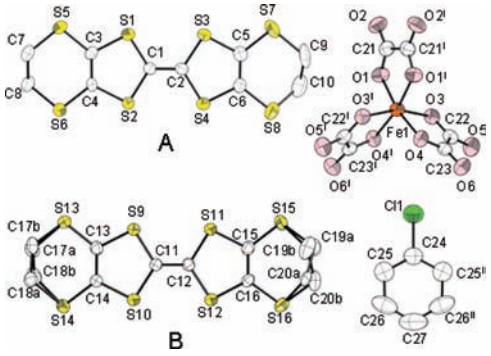

Figure 1. Thermal ellipsoid diagram (50%) of the molecules in compound **2** at room temperature. The atom numbering scheme for the isostructural salts **1**, **3**, and **4** is similar. The oxygen atom of the hydronium ion in **1**, **2**, and **3** (not shown) is labeled as O1W, while the potassium ion in **4** is labeled as K1. Symmetry codes: (i) $-x+2$, y, $-z+1/2$; (ii) $-x+1$, y, $-z+1/2$.

The crystal structures consist of alternating layers of ET molecules adopting the β'' phase and anionic layers containing $[Fe(C_2O_4)_3]^{3-}$ anions and H_3O^+ (in **1**−**3**) or K^+ cations (in **4**) with a honeycomb arrangement that leaves hexagonal cavities which are occupied by the halobenzene guest molecules (see Figure 2). In all the salts the halogen substituent is pointing toward a vertex of the hexagon occupied by a Fe(III) ion. Moreover, although the 2-fold axis of the halobenzene guest molecule lies exactly on the plane of the hexagonal cavity, the molecular plane is not parallel to the plane of the hexagonal cavity, as shown by the δ angle (Figure 3).

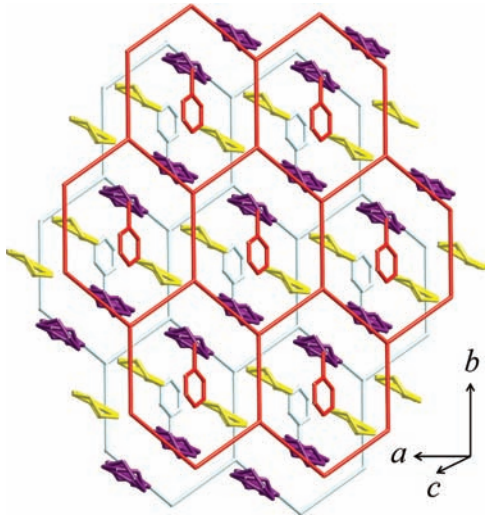

Figure 2. Projection of one of the ET layers in **1** sandwiched between two schematic inorganic layers depicted in red (top layer) and light blue (bottom layer). A and B-type ET molecules are depicted in yellow and violet, respectively.

The structural differences observed in these hexagonal units in compounds **1**−**4** can be studied in detail from the distances listed in Table 4 and graphically represented in Figures 3 and 4.

dx.doi.org/10.1021/ic202269x | Inorg. Chem. 2012, 51, 1111−1126

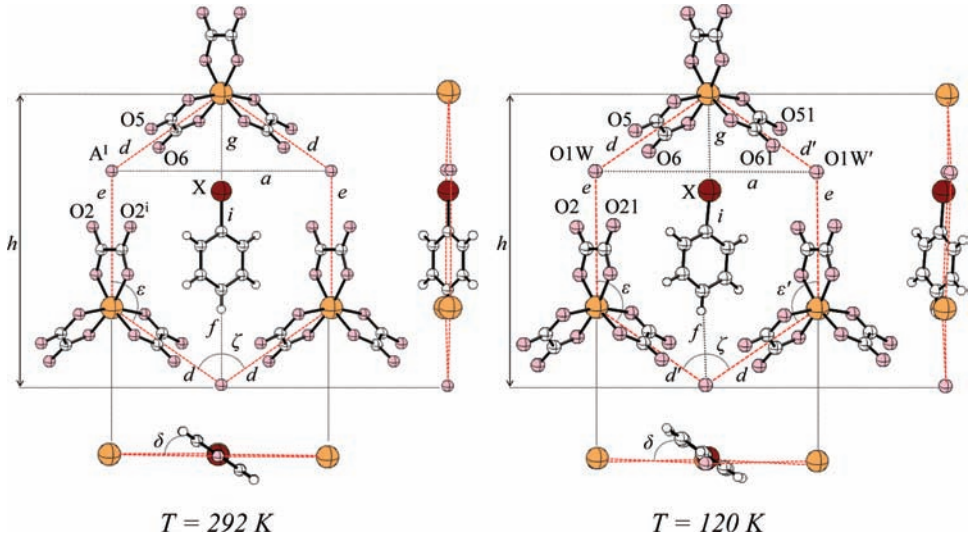

Figure 3. Front and side views of a hexagonal unit of the anionic layer of **1**−**4** at room temperature (left) and of **1**−**3** at 120 K (right).

Table 4. Selected Distances (in Å) Occurring Inside the Hexagonal Units Shown in Figure 3 for Compounds 1−4 at Room Temperature and at 120(2) K

	room temperature				T = 120 K			
	1	**2**	**3**	**4**	**1**	**2**	**3**	**4**
a (Å)	10.3123(2)	10.2899(4)	10.2875(3)	10.2260(2)	10.2595(3)	10.25276(14)	10.25554(17)	10.1637(3)
d (Å)	6.294(2)	6.288(3)	6.299(3)	6.2608(10)	6.333(14)	6.294(10)	6.322(16)	6.2197(5)
d' (Å)					6.158(14)	6.207(10)	6.207(16)	
e (Å)	6.401(4)	6.399(6)	6.392(5)	6.3485(17)	6.334(15)	6.339(10)	6.336(15)	6.2766(9)
f (Å)	4.662(9)	4.510(11)	4.472(9)	4.303(9)	4.60(3)	4.499(17)	4.42(5)	4.189(5)
g (Å)	4.942(7)	4.638(3)	4.5837(11)	4.4802(10)	4.818(19)	4.527(4)	4.500(3)	4.4334(5)
h (Å)	13.620(4)	13.627(9)	13.663(5)	13.5749(17)	13.448(15)	13.478(10)	13.524(15)	13.4485(9)
i (Å)	1.362(9)	1.752(8)	1.902(6)	2.078(7)	1.42(3)	1.763(14)	1.92(2)	2.083(4)
δ (deg)	32.83(14)	32.84(18)	33.42(16)	34.34(16)	31.5(4)	32.5(3)	33.2(4)	34.80(8)
ε (deg)	124.99(3)	125.09(4)	125.25(3)	125.25(1)	123.15(2)	123.94(15)	123.9(3)	125.21(1)
ζ (deg)	110.01(6)	109.82(8)	109.50(7)	109.50(3)	110.4(2)	110.19(14)	109.9(2)	109.58(1)
ε' (deg)					126.2(2)	125.56(15)	126.0(3)	
[a]A^{I}···O2	2.975(4)	2.967(6)	2.965(5)	2.906(4)	2.95(2)	2.945(14)	2.95(2)	2.8463(19)
A^{I}···O5	2.927(4)	2.952(5)	2.973(4)	2.942(4)	3.01(3)	2.953(15)	2.96(2)	2.9128(18)
A^{I}···O6	2.850(3)	2.826(4)	2.827(3)	2.758(4)	2.964(17)	2.873(12)	2.876(19)	2.7191(17)
A^{I}···O21					2.90(2)	2.896(13)	2.90(2)	
A^{I}···O51					2.82(2)	2.875(14)	2.89(2)	
A^{I}···O61					2.726(17)	2.780(12)	2.750(19)	
A^{I}···X	5.325(2)	5.2458(11)	5.2304(8)	5.1860(3)	5.31(2)	5.340(10)	5.375(16)	5.1520(2)
O1W···X					5.27(2)	5.106(10)	5.052(16)	

[a]A^{I} stands for O1W in compounds **1**, **2**, and **3** and K1 in compound **4**.

First of all, we observe that the dimension of the hexagonal cavity changes very little when going from **1** to **4**, emphasizing the rigidity of the inorganic sublattice. Thus, distances e and d (the sides of the hexagon) and distance a (shortest width of the hexagon) remain unchanged when going from PhF to PhBr (**1** to **3**) and decrease for compound **4** (PhI) because of changes in the interactions between the terminal oxygen atoms of the tris(oxalato)ferrate anion and the monovalent cation, which are stronger for A = K^+ (in **4**) than for A = H_3O^+ (in **1**−**3**) (Table 4). The only noticeable change occurs in the longest diagonal of the hexagon (h in Figures 3 and 4), which slightly increases from **1** to **3** because of the increase of the size of the guest molecule as X changes from F to Br, but decreases for compound **4** because of the decrease already mentioned in the distances e and d when A = K^+. The big differences between the values of the angles around the Fe^{III} and A^+ cations (ε and ζ, respectively) clearly indicate that the hexagonal cavities are flattened along the a direction ($\varepsilon > \zeta$). This distortion is also observed in some of the O−Fe−O bond angles in the tris(oxalato)ferrate(III) anion that change to follow the flattening of the hexagonal cavity (see Supporting Information).

Concerning the relative position of the guest molecules inside the cavity in compounds **1**−**4**, the increase in the C-X bond distance (i in Figures 3 and 4) when going from F to I, results in a shortening of the X···Fe and *para*-C···A distances (g and f, respectively, in Figures 3 and 4). Therefore, as expected, the increase in the size of the guest molecule reduces the free space in the hexagonal cavity since it cannot expand freely to accommodate the guest. This fact is clearly demonstrated by a well-defined decrease in g and f as we go from **1** to **4**, while the

dx.doi.org/10.1021/ic202269x | Inorg. Chem. 2012, 51, 1111−1126

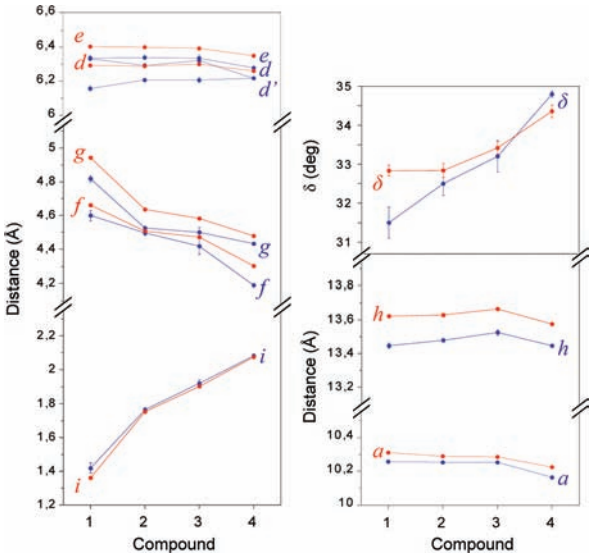

Figure 4. Graphical representation of some selected distances and angles, including error bars, of the hexagonal unit shown in Figure 3. The room temperature data are represented in red and the data at 120 K are represented in blue.

dimensions of the hexagonal cavity (*e* and *d* distances, for example, see Table 4) remain almost unaffected. The change in the relative position of the halogen atoms inside the hexagonal cavity as we go from **1** to **4** affects the interactions with the ethylene groups of the ET donors as well as the angle formed by the molecular planes of the ET molecules and the plane of the inorganic layers (see below).

Another striking structural difference is observed in the value of the angle δ formed between the plane of the phenyl ring and the plane of the hexagonal cavity, which clearly increases from **1** to **4** (Figure 4). Since this angle is closely related with the dimension of the cavity (Figure 3), then the increase observed in the δ angle has to be mainly attributed to changes in the interlayer interactions. This result supports the idea that the X atom interacts with the ET layer (more precisely, with the H atoms of the ethylene groups of the ET molecules, see below). Interestingly, as we move from I to F, the interaction is expected to be stronger, leading to a shorter distance between the organic and inorganic layers (as shown by the decrease in the *c* unit cell parameter when going from I to F, Table 4) and to a smaller δ angle (the phenyl ring rotates). Although the decrease in the interlayer distance, (related to *c*), could be attributed to a decrease in the halogen size when going from I to F, this is not the case since the tris(oxalato)ferrate anion is much wider than the halogen atom and, therefore, the steric effect exerted by the tris(oxalate)ferrate anion is expected to be dominant. This is also supported by the fact that the decrease in the *c* parameter: 14 pm (between **2** and **1**), 10 pm (between **3** and **2**) and 39 pm (between **4** and **3**) is not parallel to the differences in the van der Waals radii of the corresponding halogens: 28 pm (between Cl and F), 10 pm (between Br and Cl) and 13 pm (between I and Br).[79]

Another consequence of this expansion in the interlayer distance when passing from F to I is an increase in the angle formed between the mean plane of the ET molecules and the plane of the inorganic layers. For the A-type ET molecule the values clearly confirm this trend (69.60(1)°, 69.85(3)°, 69.92(1)° and 71.01(1)° for **1**–**4**, respectively). However for the B-type ET molecule this angle remains almost constant from **1** to **3** (67.75(1)°, 67.81(3)° and 67.76(1)°, respectively) and increases in compound **4** (68.75(1)°). The reason for this trend is that molecule B forms short contacts of the type C–H···X with the guest molecule, and, therefore, the angle that forms with the plane of the inorganic layer depends on the relative position of the halogen atom in the hexagonal cavity (i.e., the value of the *g* distance). Thus, the expected effect of the decrease in the interlayer distance when passing from I to F is partially compensated by the change in the *g* distance. In contrast, the variation of the angles formed by molecule A parallels the variation of the *c* crystallographic axis since this molecule does not form H-bonds with the guest molecule.

Let us now focus on the organic sublattice and, in particular, on the influence of the inorganic sublattice on the intermolecular S···S contacts and ethylene conformations. As previously mentioned, the ET molecules adopt a β'' packing and, as usually observed in this phase, intermolecular S···S contacts shorter than the sum of the van der Waals radii take place between molecules belonging to adjacent chains.[80] These S···S distances follow a general trend to decrease as we go from **1** to **4** (Table 5), in agreement with the progressive flattening of the hexagonal cavity in the *a* direction when passing from **1** to **4** (Figure 4). This reduction in the *a* parameter acts as a chemical pressure, slightly approaching the adjacent ET chains. In fact, the largest decrease of the intermolecular S···S distances takes place when we go from **3** to **4** (where the reduction in the *a* parameter is the biggest one), whereas the smaller decrease is observed when we go from **2** to **3** (where the reduction in *a* is smaller).

Interestingly, one of the S···S contacts (S14···S16, Table 5) follows the opposite trend and increases as we go from **1** to **3**. This contact takes place between two B-type molecules that form weak H-bonds with the halogen atoms through one of its ethylene groups. As the size of the halogen atom increases, the H···X distance also increases resulting in a slight displacement of the B-type ET molecules toward the neighboring inorganic layer (in the direction of the arrows in Figure 5). Since the two adjacent B-type molecules are pushed in opposite directions, the final effect is an increase of the S14···S16 distance as we go from **1** to **3** (Table 5). In **4**, however, the S14···S16 distance decreases because the previous effect is compensated with the larger decrease in the *a* parameter observed in this compound (Figure 4).

Concerning the order/disorder of the peripheral ethylene groups, we notice that at room temperature the four compounds have the ethylene groups of the two sides of the A-type molecules fully ordered (Figure 1) with half-chair (in the C7–C8 side) and sofa (in the C9–C10 side) conformations (Scheme 1).[81] In contrast, the B-type molecules have both ethylene groups disordered in two different positions having conformations of half-chair and sofa for the C17–C18 side and boat for both disordered conformations in the C19–C20 side. All ethylene groups form short contacts of the type C–H···O with the oxygen atoms of the oxalato ligands but only the C19–C20 ethylene is near the halogen atom of the guest molecule and forms short contacts of the type C–H···X (see Table 6 for a complete list of all these contacts). The boat conformation is probably not intrinsically stable,[82] and therefore this conformation seems to be supported by the steric effect exerted by the halogen atom of the guest molecule. The occupancy factor of 1 of the two disordered boat conformations (C19A-C20A) increases from 56% in **1** to 75% in **4**, that is, this side of the molecule becomes increasingly ordered as the size of the

dx.doi.org/10.1021/ic202269x | *Inorg. Chem.* 2012, 51, 1111–1126

Table 5. Intermolecular S···S Distances (in Å) Shorter than the Sum of the van der Waals Radii (3.60 Å) for Compounds 1−4 at Room Temperature

ET molecules	interaction[a]	1	2	3	4
A···B	S(2)···S(13)	3.3835(11)	3.3703(18)	3.3739(16)	3.3474(16)
	S(5)···S(15)^{i}	3.6159(12)[b]	3.599(2)	3.5926(16)	3.5741(18)
	S(6)···S(13)	3.3552(10)	3.3310(17)	3.3265(14)	3.2770(17)
	S(8)···S(11)	3.5492(12)	3.5430(18)	3.5392(16)	3.5214(17)
	S(8)···S(15)	3.6409(11)[b]	3.6021(18)[b]	3.5810(16)	3.5369(17)
B···B	S(10)···S(16)^{ii}	3.5394(11)	3.5182(18)	3.5131(15)	3.4785(16)
	S(14)···S(16)^{ii}	3.4015(11)	3.4180(16)	3.4391(14)	3.4147(16)

[a]Symmetry codes: (i) $-x+1/2, -y+1/2, -z$; (ii) $-x+2, -y, -z$. [b]Some distances larger than 3.60 Å are included to compare with the analogous distances of the other members of the series that are shorter than 3.60 Å.

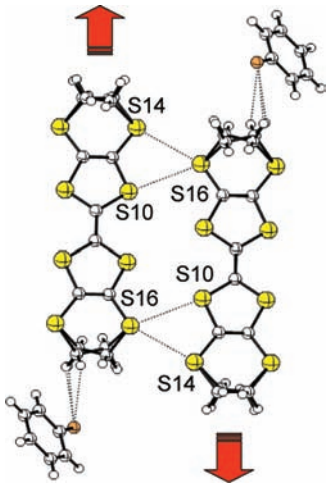

Figure 5. Two B-type ET molecules of adjacent chains in the structure of compound **1** at room temperature. Dotted lines represent short intermolecular contacts. The arrows indicate the displacement direction of the ET molecules as the halogen atom of the guest molecule passes from F to I.

Scheme 1. Three Possible Conformations Adopted by the Six-Membered Rings of the ET Molecule

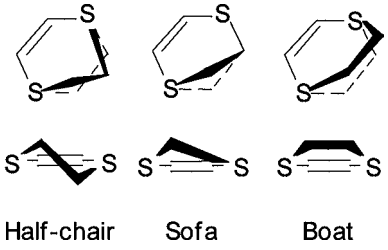

halogen atom increases, while the occupancy factors of the other disordered side of the molecule remain almost constant (between 63% and 68% for C17A-C18A, see Table 6). As expected, the boat conformation that increases its occupancy factor as the size of X increases is the one exhibiting the shortest C−H···X and C−H···O contacts, and in both boat conformations of the C19−C20 group the distances increase as the size of X increases. In contrast, the C−H···O contacts involving the other side of the molecule (C17−C18) decrease from **1** to **4**, in agreement with the fact that the B-type molecule is being progressively pushed away from the guest molecule as we go from **1** to **4**, toward the neighboring inorganic layer near the C17−C18 ethylene group (Figure 5). Concerning the C−H···O distances involving molecule A, all of them increase as we go from **1** to **4**, in parallel with the increase of the interlayer separation (c axis).

The estimation of the ionic charges on the ET molecules from the known correlations between the intramolecular bond distances of the central TTF skeleton and the oxidation degree[83] indicates that both types of ET molecules have similar charges, close to 0.5, for all compounds, in agreement with the stoichiometry of the radical salts.

Crystal Structures of $ET_4[(H_3O)Fe(C_2O_4)_3]\cdot G$ [G = PhF (1), PhCl (2), and PhBr (3)] at 120 K. Figure 6 shows the variation of the unit cell parameters of a single crystal of compound **3** as the temperature is lowered from room temperature to 120 K. Upon cooling, both α and γ angles exhibit values very close to 90° down to approximately 200 K, and below this temperature α increases while γ decreases. In contrast, the β angle increases when lowering the temperature, reaching a maximum at 170−150 K. Finally, the a, b, and c parameters follow the expected trend to contract upon cooling. These data suggests that compound **3** suffers a gradual structural transition to a lower symmetry phase with a critical temperature of about 200 K, corresponding to the splitting of the α and γ angles. Below this temperature the unit cell can no longer be considered as monoclinic, so it is better described by the triclinic reduced (or Niggli) cell obtained by applying the matrix 1, 0, 0/0.5, −0.5, 0/0, 0, −1. Compounds **1** and **2** also suffer this transition as evidenced by their unit cells at 120 K (crystal data for all compounds at 120 K are shown in Table 3). The high final R factors of the structure solutions of **1**, **2**, and **3** at 120 K are due to the problems exhibited by the diffraction patterns at this temperature (see experimental part) and therefore the crystal structures presented in this section can be considered as "average" structures.

Because of the lower symmetry ($P\bar{1}$) of the structures at 120 K, the asymmetric unit of compounds **1**−**3** doubles the one found in the structures at room temperature. Therefore, it contains four independent ET molecules (labeled as A_I, B_I, A_{II}, and B_{II}), one tris(oxalato)ferrate anion, one halobenzene molecule, and one hydronium cation (Figure 7).

Overall, the crystal structures at 120 K are similar to the structures at room temperature and maintain the same general features. At 120 K, however, the hexagonal cavities created by the anionic layers containing $[Fe(C_2O_4)_3]^{3-}$ anions and H_3O^+ cations are somewhat more distorted as a consequence of the loss of the 2-fold rotation symmetry axis, and thus, they present three different sides instead of two, (e, d, and d') and three different angles (ε, ε', and ζ) (Figure 3, right). As observed at room temperature, the values of these angles reflect the large changes in some of the O−Fe−O angles of the tris(oxalato)-ferrate anions required to accommodate the distortion of the hexagonal cavity (see Supporting Information). As expected, all

dx.doi.org/10.1021/ic202269x | Inorg. Chem. 2012, 51, 1111−1126

Table 6. Intermolecular C−H···O and C−H···X Distances (in Å) Shorter than the Sum of the van der Waals Radii for 1−4 at Room Temperature[a]

ET molecule	conformation	interaction[b]	1	2	3	4
ET-A	half-chair	C8−H8B···O1^{i}	2.61	2.61	2.64	2.68
		C8−H8B···O4^{ii}	2.68	2.74	2.76	2.79
	sofa	C10−H10A···O2^{iii}	2.43	2.46	2.48	2.49
ET-B	half-chair	C17A−H17B···O5^{i}	2.43 (63%)	2.42 (66%)	2.40 (68%)	2.50 (66%)
		C18A−H18B···O6	2.56	2.48	2.44	2.38
	sofa	C17B−H17C···O5^{i}	2.47 (37%)	2.55 (34%)	2.58 (32%)	2.57 (34%)
		C18B−H18C···O6	2.62	2.52	2.53	2.40
	boat	C19A−H19A···X^{iv}	2.96 (56%)	2.98 (63%)	3.02 (67%)	3.11 (75%)
		C19A−H19B···X^{iv}	2.94	3.04	3.11	3.20
		C20A−H20A···O4^{v}	2.35	2.45	2.50	2.64
	boat	C19B−H19C···O5^{vi}	2.49 (44%)	2.38 (37%)	2.41 (33%)	2.45 (25%)
		C19B−H19D···O5^{vi}	2.83	2.76	2.70	2.64
		C19B−H19D···X^{iv}	3.00	3.00	3.09	3.16
		C20B−H20D···O4^{v}	2.49	2.51	2.55	2.68

[a]The conformation of each ethylene group is also indicated as well as their percentage of occupation when disordered. Some longer distances are included for comparison with the analogous distances of other members of the series that are shorter than the sum of the van der Waals radii. [b]Symmetry codes: (i) 1−*x*, *y*, 1/2−*z*; (ii) −1+*x*, *y*, *z*; (iii) −1/2+*x*, 1/2−*y*, −1/2+*z*; (iv) 3/2−*x*, 1/2−*y*, −*z*; (v) 2−*x*, −*y*, −*z*; (vi) *x*, −*y*, −1/2+*z*. The van der Waals radii are: C = 1.70, H = 1.20, O = 1.52, F = 1.47, Cl = 1.75, Br = 1.85, and I = 1.98 Å.

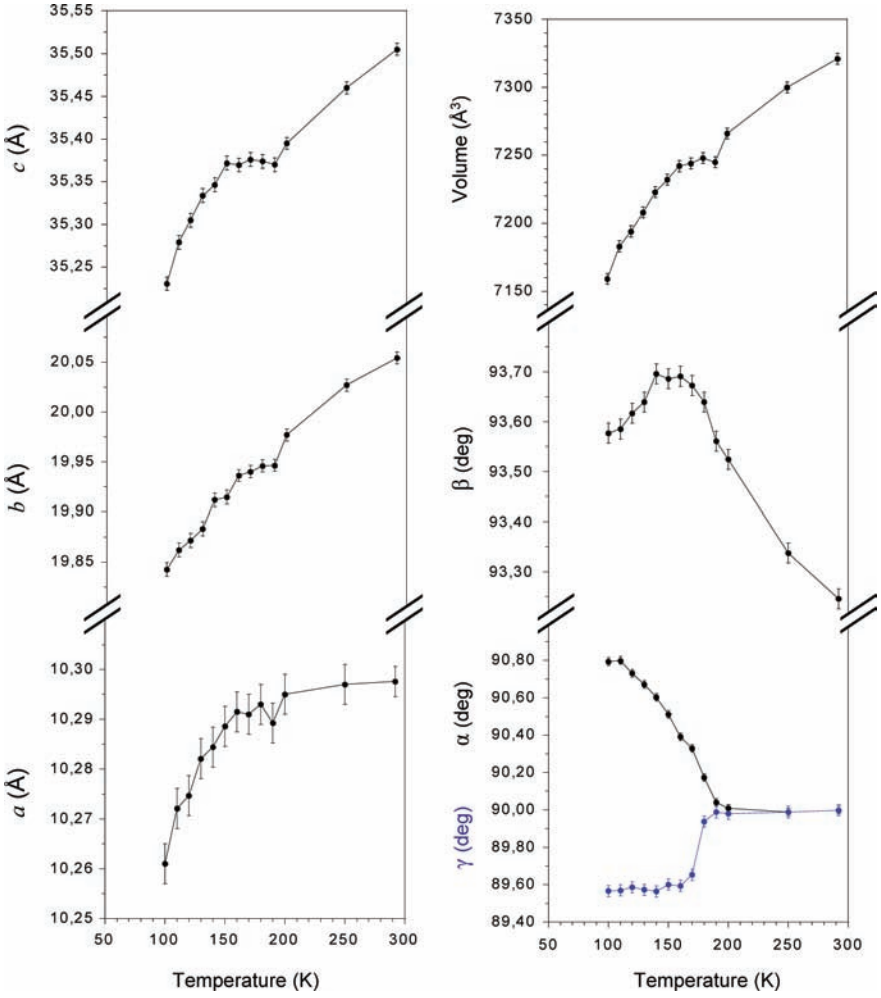

Figure 6. Variation of the unit cell parameters of a single crystal of compound **3** on cooling from 292(2) to 100(2) K determined by single-crystal X-ray diffraction. The single-crystal used for this experiment was different to the one used for the structure determination at 120 K.

the intermolecular distances defining the geometry of the hexagonal cavities are shortened at 120 K with respect to the room temperature values. In any case, these intermolecular distances follow the same trends as the ones observed at room temperature when we go from **1** to **3** (and even for **4**, whose structure is discussed in the next section), as can be seen in

dx.doi.org/10.1021/ic202269x | *Inorg. Chem.* 2012, 51, 1111−1126

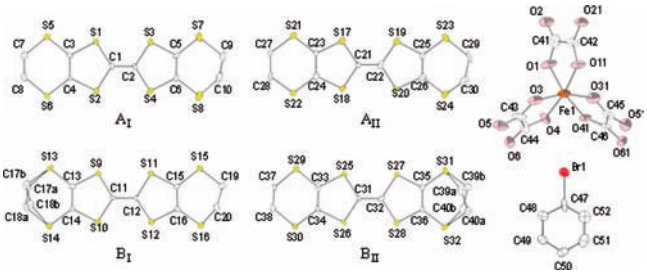

Figure 7. Thermal ellipsoid diagram (50%) of the molecules in compound **3** at 120 K. The atom numbering scheme for the isostructural salts **1** and **2** is similar.

Figure 4. Still, the most noticeable structural change concerns the guest molecule. On one hand, the main axis of the halobenzene molecule, which at room temperature was directed along the longest diagonal of the hexagon, is now slightly tilted by about 2.5, 3.8 and 4.6° in compounds **1**−**3**, respectively, (measured as the projection of the C-X bond into the hexagonal layer, Figure 3). As expected, these angles increase as we pass from F to Cl and Br. The distances from the halogen atom to the two nearest hydronium ions in the hexagonal cavity (Table 4) indicate that the tilt is slightly more pronounced as the size of the halogen atom increases (the asymmetry, measured by the difference between these two distances, is 4, 23, and 32 pm in **1**−**3**, respectively). On the other hand, the main axis of the halobenzene molecule slightly separates from the plane of the hexagonal cavity in such a way that the *para* carbon atom is more separated from the plane than the halogen atom (Figure 3.right). The distances from these two atoms to the plane of the cavity are similar for all three compounds (0.51(3) and 0.218(19) Å for **1**, 0.515(16) and 0.195(6) Å for **2** and 0.42(2) and 0.174(9) Å for **3**). As a consequence of this displacement, the guest molecule is nearer to the ET molecules of one layer than to those of the adjacent layer, resulting in two nonequivalent ET layers (labeled as I and II in Figure 8). Each

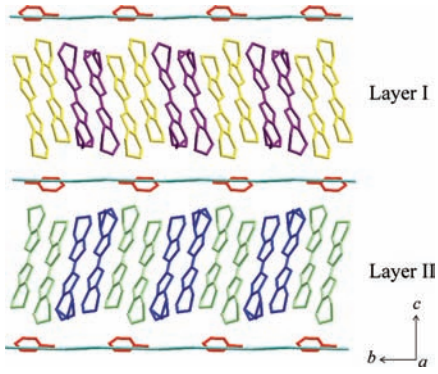

Figure 8. Projection of the structure of **1** at 120 K showing the two nonequivalent organic layers arising from the displacements of the guest molecules that now are closer to the ET molecules of layer II than of layer I. The crystallographically independent ET molecules are depicted in different colors (A_I in yellow, B_I in violet, A_{II} in light green, and B_{II} in dark blue). The light blue lines represent the average planes of the inorganic layers.

of these layers is built with two crystallographically independent ET molecules (A_I and B_I for layer I and A_{II} and B_{II} for layer II), see Figure 8, coming from the A and B-type ET molecules at room temperature by effect of the loss of symmetry.

It is worth noting that, while the A_I and A_{II} molecules have all their ethylene groups ordered (as their counterpart molecule of type A at room temperature), molecules B_I and B_{II} have only one ethylene group disordered, compared to molecule B at room temperature where both ethylene groups are disordered. Therefore, a partial ordering process of the ethylene groups takes place on cooling (only 25% of the ethylene groups are disordered at 120 K compared with 50% at room temperature). Moreover, the ethylene groups of B_I and B_{II} that become ordered at 120 K are located on opposite sides: in B_I it is the one interacting with the halogen atom of the guest molecule (C19−C20), while in B_{II} the ordered ethylene group is the one located on the opposite side and far from the guest molecule (C37−C38). This behavior cannot be definitely explained in terms of the intermolecular C−H···X or C−H···O contacts, given the high standard deviations in the structures at 120 K. On the other hand, the ethylene groups at 120 K adopt the same conformations exhibited by the ethylene groups from which they come from at room temperature.

Table 7 shows the intermolecular S···S distances shorter than the sum of the van der Waals radii in **1**, **2**, and **3** at 120 K. As

Table 7. Intermolecular S···S Distances (in Å) Shorter than the Sum of the van der Waals Radii (3.60 Å)[a] for 1−3 at 120 K

ET molecules	interaction[c]	1	2	3
A_I···B_I	S2···S13^{i}	3.321(4)	3.315(3)	3.323(5)
	S5···S15	3.608(4)	3.597(3)	3.576(6)
	S6···S13^{i}	3.290(4)	3.279(3)	3.286(5)
	S8···S11^{i}	3.536(5)	3.549(3)	3.530(5)
	S8···S15^{i}	3.598(4)	3.568(3)	3.547(5)
	[b]S8···S14^{ii}	3.588(5)	3.594(4)	3.598(6)
B_I···B_I	S10···S16^{iii}	3.486(4)	3.496(3)	3.485(5)
	S14···S16^{iii}	3.376(4)	3.395(3)	3.400(5)
A_{II}···B_{II}	S18···S29	3.381(4)	3.373(3)	3.369(5)
	S21···S31^{v}	3.561(5)	3.535(3)	3.541(6)
	S22···S29	3.336(4)	3.316(3)	3.313(5)
	S24···S27	3.404(4)	3.412(3)	3.433(5)
	S24···S31	3.537(4)	3.518(3)	3.521(5)
	[b]S24···S30^{vi}	3.585(5)	3.602(3)	3.616(5)
	[b]S19···S32^{iv}	3.602(4)	3.588(3)	3.592(5)
B_{II}···B_{II}	S26···S32^{vii}	3.435(4)	3.403(3)	3.408(5)
	S30···S32^{vii}	3.340(4)	3.362(3)	3.391(5)

[a]Some contacts larger than 3.60 Å are included for comparison with analogous distances of other member of the series that are shorter than 3.60 Å. [b]These contacts were not present in the room temperature crystal structure. [c]Symmetry codes: (i) $-x, -y+1, -z+2$; (ii) $x-1, y+1, z$; (iii) $-x+2, -y, -z+2$; (iv) $x-1, y, z$; (v) $-x+1, -y+1, -z+1$; (vi) $-x+1, -y+2, -z+1$; (vii) $-x+2, -y+2, -z+1$.

expected, they are shorter and more abundant than the corresponding contacts at room temperature. However, the higher standard deviations compared to those in the room temperature data prevent one from unraveling any possible trends existing in these distances as we go from **1** to **3**. An estimation of the ionic charges of the ET molecules at 120 K from the bond lengths of the central TTF skeletons is inappropriate for the same reasons.

Crystal Structure of $ET_4[KFe(C_2O_4)_3]\cdot PhI$ (4) at 120 K. Compound **4** does not undergo the structural transition described in the previous section for **1**, **2**, and **3**, at least for temperatures above 120 K. Therefore, the crystal structure of **4** at 120 K can be described in the monoclinic space group $C2/c$, as it was at room temperature (Table 3).

As can be seen in Table 4 and in Figure 4, all the intermolecular distances represented in the left side of Figure 3 have

dx.doi.org/10.1021/ic202269x | *Inorg. Chem.* 2012, 51, 1111−1126

shortened and therefore the hexagonal cavities are slightly smaller at 120 K than at room temperature, although they keep the same distortion, as indicated by the values of the ε and ζ angles, which remain unchanged at both temperatures. This shortening of the dimensions of the hexagonal units, in particular the shortening of its shortest width (represented by the *a* parameter), accounts for the increase of the angle between the guest molecule and the hexagonal planes (δ) at 120 K with respect to the room temperature value. However, the values of the δ angle for **1**, **2**, and **3** are smaller at 120 K than at room temperature because in these structures the guest molecule separates from the plane of the hexagonal cavity and is tilted with respect to the longest diameter of the hexagon (see previous section). As expected from the reduction of the dimensions of the hexagonal cavity, all the intermolecular S···S distances are also shortened at 120 K and, therefore, there are more S···S contacts shorter than the sum of the van der Waals radii than at room temperature (Table 8).

Table 8. Intermolecular S···S Distances (in Å) Shorter than the Sum of the van der Waals Radii (3.60 Å)[a] in 4 at 292 and 120 K

ET molecules	interaction[b]	292 K	120 K
A···B	S(2)···S(13)	3.3474(16)	3.3058(7)
	S(5)···S(15)^{i}	3.5741(18)	3.5239(8)
	S(6)···S(13)	3.2770(17)	3.2384(7)
	S(8)···S(11)	3.5214(17)	3.4443(7)
	S(8)···S(15)	3.5369(17)	3.4342(8)
	S(3)···S(5)^{iii}	3.6255(16)	3.5928(7)
	S(3)···S(16)^{iv}	3.6581(17)	3.5954(8)
	S(8)···S(14)^{v}	3.6281(17)	3.5877(8)
B···B	S(10)···S(16)^{ii}	3.4785(16)	3.4290(7)
	S(14)···S(16)^{ii}	3.4147(16)	3.3741(7)

[a]Some contacts larger than 3.60 Å are included at room temperature for comparison with the analogous distances at 120 K that are shorter than 3.60 Å. [b]Symmetry codes: (i) $-x+1/2, -y+1/2, -z$; (ii) $-x+2, -y, -z$; (iii) $-x-1/2, -y+1/2, -z$; (iv) $x-1, y, z$; (v) $-x+1, -y, -z$.

The distance between different inorganic layers (represented by half the value of the crystallographic *c* axis) is also smaller at 120 K than at room temperature (the *c* values are 35.9064(4) and 35.6405(11) Å, at 292 and 120 K, respectively, Table 3). This reduction in the *c* parameter produces a logical decrease of the angles formed by the planes of the ET molecules and the plane of the inorganic layer since now there is less space (the angles are 71.02(1)° and 68.75(1)° for molecules A and B, respectively, at room temperature, and 70.36(1)° and 67.98(1)° for molecules A and B at 120 K).

The conformations adopted by the ethylene groups of the ET molecules are the same at 120 K than at room temperature, and the weak H-bonds of the type C−H···O and C−H···I established with the inorganic layer are also essentially similar at both temperatures (see Table 9). The most significant difference with respect to the crystal structure at room temperature is the higher degree of ordering in the ethylene groups of the B-type molecule. For example, in the ethylene group that interacts with the halogen atom, the occupancy factor of one of the disordered boat conformations (C19A-C20A, the one forming the shortest C−H···I contacts) increases from 75% at room temperature, to 91% at 120 K (Table 9).

Table 9. Intermolecular C−H···O and C−H···X Distances (in Å) Shorter than the Sum of the van der Waals Radii[a] in 4 at 292 and 120 K[b]

ET molecule	conformation	interaction[c]	292 K	120 K
ET-A	half-chair	C8−H8B···O1^{i}	2.68	2.68
		C8−H8B···O4^{ii}	2.79	2.75
	sofa	C10−H10A···O2^{iii}	2.49	2.44
ET-B	half-chair	C17A−H17B···O5^{i}	2.50 (66%)	2.42 (87%)
		C18A−H18B···O6	2.38	2.33
	sofa	C17B−H17C···O5^{i}	2.57 (34%)	2.51 (13%)
		C18B−H18C···O6	2.40	2.38
	boat	C19A−H19A···X^{iv}	3.11 (75%)	3.08 (91%)
		C19A−H19B···X^{iv}	3.20	3.17
		C20A−H20A···O4^{v}	2.64	2.55
		C19A−H19A···O5^{vi}	2.76	2.65
	boat	C19B−H19C···O5^{vi}	2.45 (25%)	2.40 (9%)
		C19B−H19D···O5^{vi}	2.64	2.38
		C19B−H19D···X^{iv}	3.16	3.18
		C20B−H20D···O4^{v}	2.68	2.56

[a]Some longer distances are included for comparison with the analogous distances of other members of the series that are shorter than the sum of the van der Waals radii. [b]The conformation of each ethylene group is also indicated as well as their percentage of occupation when disordered. [c]Symmetry codes: (i) $1-x, y, 1/2-z$; (ii) $-1+x, y, z$; (iii) $-1/2+x, 1/2-y, -1/2+z$; (iv) $3/2-x, 1/2-y, -z$; (v) $2-x, -y, -z$; (vi) $x, -y, -1/2+z$. The van der Waals radii are C = 1.70, H = 1.20, O = 1.52, F = 1.47, Cl = 1.75, Br = 1.85, and I = 1.98 Å.

The analysis of the intramolecular bond distances of the ET molecules indicates that the charge distribution in the organic sublattice is very similar at 120 K and at room temperature, that is, both ET molecules bear a charge close to 0.5.

Electrical Properties. The dc electrical conductivity measurements, performed on several single crystals of each compound, show that the three salts with A = H_3O^+ (**1**−**3**) are metallic and show similar thermal dependences: the resistivity decreases as the sample is cooled to reach a broad minimum at about 180, 95, and 80 K for **1**−**3**, respectively (Figure 9). Below the minimum, the resistivity smoothly increases and reaches a maximum at low temperatures in compounds **1** and **3** (ca. 1.0

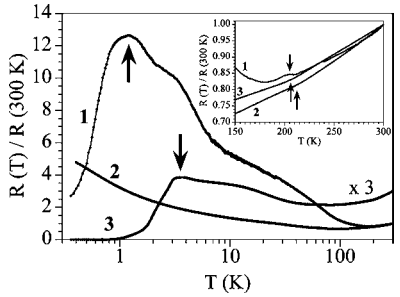

Figure 9. Thermal variation (*T* in logarithmic scale) of the normalized dc electrical resistance of compounds **1**−**3** (the normalized resistance of **3** has been multiplied by a factor of 3). Arrows indicate the onset of the superconducting transitions in **1** and **3**. Inset shows the high temperature region (*T* in linear scale). Arrows indicate the tiny changes in the slopes at about 200−210 K for **1**−**3**.

and 4.0 K in **1** and **3**, respectively). Below these temperatures the resistivity shows a sharp decrease in both salts, indicative of

dx.doi.org/10.1021/ic202269x | Inorg. Chem. 2012, 51, 1111−1126

a superconducting transition. Compound **2** does not show any maximum nor a superconducting transition at temperatures above 0.4 K. As observed in other superconductors of the β'' series,[56] the two superconducting samples show a shoulder a few Kelvin above the superconducting transition (at ca. 3 and 10 K in salts **1** and **3**, respectively, Figure 9). An interesting feature shown by the three compounds is the presence of a small change in the slope of the resistivity near 200−210 K (inset in Figure 9). This tiny change may be due to the structural transition discussed above. Note that since this structural transition does not produce important changes in the ET layers its effect on the transport properties is also small.

Although compound **1** does not reach zero resistance above the lowest attainable temperature (0.4 K), the nature of this transition is confirmed by performing magneto-resistance measurements. Thus, when the magnetic field is applied perpendicular to the conducting layers, the resistivity shows the same behavior observed in absence of magnetic field until the field reaches a value of about 200 mT (Figure 10). Above about

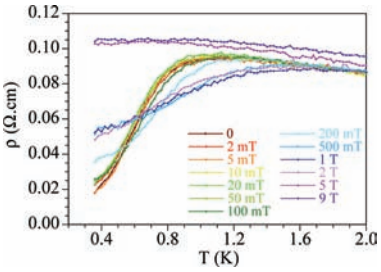

Figure 10. Thermal variation of the electrical resistivity of compound **1** under different magnetic fields applied perpendicular to the conduction plane.

200 mT the resistivity at low temperatures increases and above 5 T the transition is suppressed.

This behavior is similar to that observed in compound **3**[48] and in other superconductors of this series[8,43,56] and can be clearly confirmed in the plot of the resistivity as a function of the magnetic field at 0.4 K (Figure 11). This plot shows a sharp increase of the resistivity with increasing magnetic fields up to a value of about 0.55 T. Above this field the resistivity shows a smooth decrease to reach a minimum at about 1.7 T and increases again up to a value of about 4.5 T. Above this field the resistivity remains constant, and the superconducting transition is suppressed. A close look at the low field data (inset in Figure 11) shows that initially the resistivity slightly decreases when the magnetic field increases and reaches a broad minimum at about 20 mT. This behavior is also observed in the PhBr derivative (**3**) when the magnetic field is applied parallel to the conducting layers, although the minimum is reached at lower fields (5 mT, Supporting Information, Figure S1). Interestingly, this phenomenon is also observed in the two other superconducting salts with bromobenzene guest molecules: $ET_4[(H_3O)M(C_2O_4)_3]\cdot PhBr$ (M^{III} = Cr and Mn),[51] where the minima are observed at 4.5 and 2.5 mT, respectively. Unfortunately, there are no detailed reports of the influence of low magnetic fields applied parallel to the conducting layer on the conducting properties of this series of paramagnetic superconductors and, therefore, we cannot compare the results observed here with other derivatives in this series. The minimum in the magneto-resistance plot can be associated to the presence of an internal field of a few mT, generated by the paramagnetic $[M(C_2O_4)_3]^{3-}$ anions (M^{III} = Fe, Cr, and Mn) that is canceled by the progressive application of an external field. When the internal field is canceled, the resistivity is expected to show a minimum value. A possible reason explaining the origin of this internal field could be the presence of localized currents in the surface of the crystal because of surface defects and inhomogeneities. Any case, this internal field cannot be attributed to a residual field in the coils of the measurement equipment because (1) it would be independent of the sample measured and (2) it appears even when the residual magnetic field is canceled and reduced to a very low value (less than 1% of the observed value).

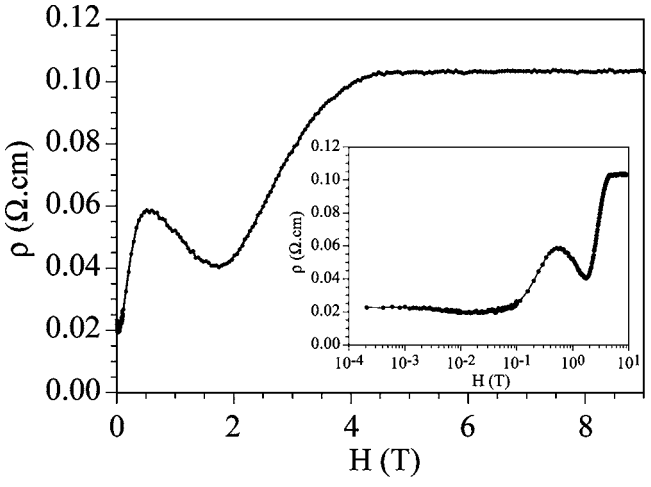

Figure 11. Electrical resistivity of compound **1** at 0.4 K as a function of the magnetic field applied parallel to the conducting layer. Inset shows the same plot in a logarithmic field scale.

A further confirmation of the nature of the superconducting transition is provided by its dependence on the current intensity that shows an increase in the resistivity for currents above about 20 μA and a suppression of the superconducting transition for currents above 50 μA in the studied sample (see Supporting Information, Figure S2).

In contrast to compounds **1**−**3**, the thermal variation of the resistivity of compound **4**, (the only one with K^+ instead of H_3O^+) shows a semiconducting behavior with a high room temperature conductivity of about 3.4 S cm^{-1} and a low activation energy of about 64 meV (Figure 12). The slight changes in the

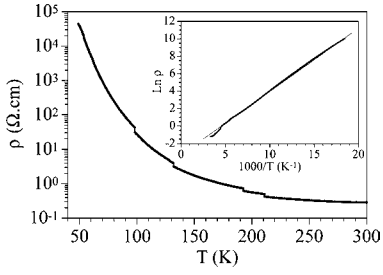

Figure 12. Thermal variation of the electrical resistivity for compound **4**. Inset shows the Arrhenius plot with the fit to a classical semiconductor model (see text).

activation energy at high temperatures are not due to any structural transition but rather to the presence of microfractures in the single crystal during the cooling scan. In fact, during the cooling scan there are small jumps in the resistivity, which are irreversible and produce irreversible increases in the activation

dx.doi.org/10.1021/ic202269x | Inorg. Chem. 2012, 51, 1111−1126

energy after these jumps. As expected, in the warming scan, since there are no further microfractures, the activation energy is similar to that found at low temperatures in the cooling scan (ca. 64 meV in the temperature range 50−300 K).

Note that this result is not surprising since all the known salts with K^+ ions in the series $ET_4[AFe(C_2O_4)_3]\cdot G$ are semiconductors (Table 1). Furthermore, as can be seen in Tables 1 and 2, to date, all the known superconducting salts contain H_3O^+ in the inorganic layer, except maybe the two salts with G = $PhNO_2$ and M = Fe and Cr, where the cation could not be unambiguously assigned.[43]

Magnetic Susceptibility. The thermal variation of the product of the magnetic susceptibility times the temperature ($\chi_m T$) shows, as expected, a similar behavior in compounds **1**−**3**. Thus, $\chi_m T$ shows a room temperature value of about 4.6−4.7 emu K mol^{-1} that decreases linearly to reach a value of about 4.2−4.3 emu K mol^{-1} at low temperatures. Compound **1** shows a small change in $\chi_m T$ between 200 and 180 K, centered at about 190 K (inset in Figure 13). This tiny change may be due to the structural transition observed at the same temperature

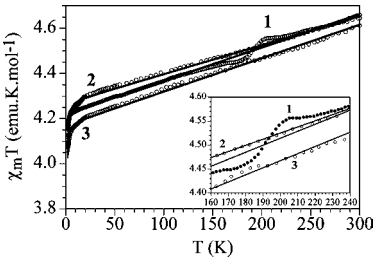

Figure 13. Thermal variation of the $\chi_m T$ product for compounds **1**−**3**. Solid lines are the best fit to the model (see text). Inset shows the high temperature region with the weak change observed in **1** centered at about 190 K.

(see above) also confirmed in the conductivity measurements. Note that this change is not an artifact since it can be reproduced in different cooling and warming scans and even shows a very small hysteresis of a few K. Below 5 K, $\chi_m T$ shows a more abrupt decrease to reach a value of about 4.1 emu K mol^{-1} at 2 K. This behavior is typical of a paramagnetic $S = 5/2$ system (the expected $\chi_m T$ value is 4.375 emu K mol^{-1} for $g = 2$) with a temperature independent paramagnetic (TIP) contribution that can be attributed to the metallic sublattice (Pauli-type paramagnetism). This TIP accounts for the linear decrease in $\chi_m T$ with decreasing temperature. The more abrupt decrease at very low temperatures can be attributed to a very weak antiferromagnetic exchange and/or to a zero field splitting (ZFS) of the isolated $S = 5/2$ Fe(III) ions. Accordingly, we have fit the magnetic behavior of compounds **1**−**3** to a simple model of an $S = 5/2$ monomer with a zero field splitting[84] plus a temperature independent term ($N\alpha$) to account for the Pauli paramagnetism. This simple model reproduces very satisfactorily the magnetic properties of compounds **1**−**3** in the whole temperature range with the following parameters: $g = 1.965$, $|D| = 0.31$ cm^{-1}, and $N\alpha = 1.5 \times 10^{-3}$ emu mol^{-1} for **1**, $g = 2.024$, $|D| = 0.65$ cm^{-1}, and $N\alpha = 1.4 \times 10^{-3}$ emu mol^{-1} for **2**, and $g = 2.001$, $|D| = 0.52$ cm^{-1}, and $N\alpha = 1.5 \times 10^{-3}$ emu mol^{-1} for **3**. Both, the g and $|D|$ values are within the normal range found in other Fe(III) $S = 5/2$ complexes.[85] Note that the sign of the $|D|$ value cannot be determined from powder magnetic susceptibility measurements and that this value may include a very weak antiferromagnetic coupling between the $[Fe(C_2O_4)_3]^{3-}$ monomers.

As mentioned above, the small change in the $\chi_m T$ product for **1** (not observed in **2** and **3**, see inset in Figure 13) may be due to a small change in the geometry of one (or both) of the $[Fe(C_2O_4)_3]^{3-}$ complexes present in the low temperature phase. Thus, although the low temperature phase could not be solved very accurately, the analysis of the Fe−O bond distances in the $[Fe(C_2O_4)_3]^{3-}$ anions shows an unexpected increase of the average Fe−O bond distance when the temperature decreases from 292 to 120 K only in the PhF derivative (**1**) whereas the two other compounds (**2** and **3**) show the expected small decrease (in **2** the decrease is within the experimental error, Table 10). Note that although the angles also vary when going from room temperature to 120 K their variations are similar in all compounds. The increase of the average Fe−O bond distance observed in **1** suggests that in this compound the displacement of the PhF molecule exerts a more important effect on the anionic layer, in agreement with the higher polarizing effect of the F atom as compared with the other halogen atoms. This different behavior of **1** as compared to **2** and **3** and the higher polarizing effect of the F atom also agrees with the fact that **1** exhibits the larger variations in the *g*, *d*, and *e* distances inside the hexagonal cavity when passing from 292 to 120 K (Figure 4 and Table 4). Note finally that although in compound **3** there is a small kink at about 190 K (inset in Figure 13) we cannot be sure that this is a true change or that it is due to the noise of the magnetic measurement.

CONCLUSIONS

We have prepared a whole series of radical salts containing halobenzenes as guest molecules formulated as $ET_4[AFe(C_2O_4)_3]\cdot G$, with A/G = H_3O^+/PhF (**1**); H_3O^+/PhCl (**2**); H_3O^+/PhBr (**3**), and K^+/PhI (**4**). These salts are isostructural

Table 10. Fe−O Bond Distances (in Å) in the $[Fe(C_2O_4)_3]^{3-}$ Anions in Compounds 1−3 at 292 and 120 K

	compound **1**		compound **2**		compound **3**	
atoms	292 K[a]	120 K	292 K[a]	120 K	292 K[a]	120 K
Fe1−O1	2.015(2)	2.009(12)	2.016(3)	2.013(8)	2.019(3)	2.029(13)
Fe1−O3	2.0079(19)	1.991(13)	2.008(3)	2.001(8)	2.011(2)	1.987(12)
Fe1−O4	2.011(2)	1.994(11)	2.013(3)	2.001(8)	2.009(3)	2.003(12)
Fe1−O11		2.019(11)		2.020(8)		1.998(13)
Fe1−O31		2.026(12)		2.019(8)		2.018(13)
Fe1−O41		2.038(11)		2.018(8)		1.995(11)
average	2.0113(11)	2.0128(5)	2.0123(17)	2.012(3)	2.0130(16)	2.005(5)

[a]There are only three different Fe−O bond distances at 292 K because of the presence of a C_2 axis passing through the Fe(III) ion.

dx.doi.org/10.1021/ic202269x | Inorg. Chem. 2012, 51, 1111−1126

at room temperature, exhibiting the well-known monoclinic $C2/c$ phase common to other members of these series containing different G molecules (Tables 1 and 2). The use of different halogen atoms in the guest molecules induces small structural changes in the organic sublattice that affect the physical properties. For example as the size of the halogen atom increases most of the intermolecular S···S distances are shorter, the angles formed by the molecular planes of the ET molecules and the anionic layer increase, and the degree of ordering of some ethylene groups is higher. When the temperature is lowered, compounds **1**, **2**, and **3** undergo a phase transition (at ∼200 K for **3**) to a triclinic phase in which there are two nonequivalent organic layers (both with β'' packing) and some ethylene groups are ordered with respect to the room temperature structure.

The analysis of the phase transition observed in compounds **1**−**3** at about 200 K with structural, electrical, and magnetic techniques allows us to draw a quite approximate description of its mechanism and its consequences on the physical properties. Thus, in the cooling scan, when the temperature reaches about 210 K, the first step is the partial ordering of some of the disordered ethylene groups of the ET molecules. This ordering starting at about 210 K is responsible for the split of the unit cell α and γ angles (Figure 6) and also for the change in the slope of the resistivity plots occurring at that temperature (inset in Figure 9). As a consequence of this ordering, there is a slight rotation of the planes of the ET molecules together with a longitudinal displacement of these ET molecules (Figure 5). This change in the ET layer induces a reduction in the size of the hexagonal cavity that pushes away the solvent halobenzene molecule, leading to a change in the local geometry of the $[Fe(C_2O_4)_3]^{3-}$ anions and resulting in a slight change in the magnetic signal (at least in the PhF derivative). The superconducting transitions observed in the PhBr and PhF derivatives but not in the PhCl one, suggests that the superconducting transition might be triggered by the ordering of the ethylene groups of the ET molecules. This ordering seems to be assisted by the C−H···X interactions (Table 6). Thus, a close look at these interactions shows that the strongest interactions are observed in the PhBr derivatives (there are three C−H···Br interactions with an average C···Br distance of 3.07 Å, that is, 0.48 Å shorter than the sum of the corresponding van der Waals radii). In contrast, the PhCl derivatives present somewhat weaker C−H···X interactions, with average C···X distances 0.44 Å shorter that the sum of the corresponding van der Waals radii. This observation agrees with the fact that in the corresponding Cr(III) salts, $ET_4[(H_3O)Cr(C_2O_4)_3]\cdot PhX$, the PhBr derivative also shows a superconducting transition (although with a lower T_c of 1.5 K) whereas the PhCl derivative does not show any superconducting transition above 0.4 K.[51] Finally, although the average C···X distance in the PhF derivative is only 0.20 Å shorter that the sum of the corresponding van der Waals radii, the ordering effect of the PhF molecule is expected to be much higher because of the strong electronegativity of the F atom. To prove this hypothesis, we are now preparing ET salts with the same PhX guest molecules but with different trivalent metal atoms as Cr^{III}, Mn^{III}, Al^{III}, and Co^{III}. This work has produced up to now two new paramagnetic superconductors, $ET_4[(H_3O)Cr(C_2O_4)_3]\cdot PhBr$ (T_c = 1.5 K) and $ET_4[H_3OMn(C_2O_4)_3]\cdot PhBr$ (T_c = 2.0 K), and a paramagnetic metal, $ET_4[(H_3O)Cr(C_2O_4)_3]\cdot PhCl$ with a $T_{M\text{-}I}$ = 130 K (Table 2). Work is in progress to include all the halobenzene molecules in these systems.

■ ASSOCIATED CONTENT

Supporting Information

Tables with bond distances in the $[Fe(C_2O_4)_3]^{3-}$ anions for compounds **1**−**4** at 298 and 120 K. Plot of the magnetoresistance of compound **3** at 0.4 K, (Figure S1), current dependence of the superconducting transition in **1** (Figure S2), and crystallographic data for compounds **1**, **2**, **3**, and **4** in CIF format at 298 and 120 K. This material is available free of charge via the Internet at http://pubs.acs.org.

■ AUTHOR INFORMATION

Corresponding Author

*E-mail: carlos.gimenez@uv.es (C.G.-S.), carlos.gomez@uv.es (C.J.G.-G.).

■ ACKNOWLEDGMENTS

We thank the EU (SPINMOL ERC Adv. Grant), the Spanish Ministerio de Ciencia e Innovacion (Projects Consolider-Ingenio in Molecular Nanoscience CSD2007-00010, MAT2007-62584 and CTQ-2011-26507) and the Generalitat Valenciana (Prometeo Program).

■ REFERENCES

(1) Coronado, E.; Day, P. *Chem. Rev.* **2004**, *104*, 5419−5448.
(2) Enoki, T.; Miyazaki, A. *Chem. Rev.* **2004**, *104*, 5449−5478.
(3) Kobayashi, H.; Cui, H.; Kobayashi, A. *Chem. Rev.* **2004**, *104*, 5265−5288.
(4) Coronado, E.; Galán-Mascarós, J. R.; Gómez-García, C. J.; Laukhin, V. *Nature* **2000**, *408*, 447−449.
(5) Coronado, E.; Martí-Gastaldo, C.; Navarro-Moratalla, E.; Ribera, A.; Blundell, S. J.; Baker, P. J. *Nat. Chem.* **2010**, *2*, 1031−1036.
(6) Kobayashi, H.; Kobayashi, A.; Cassoux, P. *Chem. Soc. Rev.* **2000**, *29*, 325−333.
(7) Graham, A. W.; Kurmoo, M.; Day, P. *J. Chem. Soc., Chem. Commun.* **1995**, 2061−2062.
(8) Kurmoo, M.; Graham, A. W.; Day, P.; Coles, S. J.; Hursthouse, M. B.; Caulfield, J. L.; Singleton, J.; Pratt, F. L.; Hayes, W. *J. Am. Chem. Soc.* **1995**, *117*, 12209−12217.
(9) Kobayashi, H.; Fujiwara, E.; Fujiwara, H.; Tanaka, H.; Tamura, I.; Bin, Z.; Gritsenko, V.; Otsuka, T.; Kobayashi, A.; Tokumoto, M.; Cassoux, P. *Mol. Cryst. Liq. Cryst.* **2002**, *379*, 9−18.
(10) Kobayashi, H.; Tomita, H.; Naito, T.; Kobayashi, A.; Sakai, F.; Watanabe, T.; Cassoux, P. *J. Am. Chem. Soc.* **1996**, *118*, 368−377.
(11) Kobayashi, H.; Fujiwara, E.; Fujiwara, H.; Tanaka, H.; Otsuka, T.; Kobayashi, A.; Tokumoto, M.; Cassoux, P. *Mol. Cryst. Liq. Cryst.* **2002**, *380*, 139−144.
(12) Fujiwara, H.; Fujiwara, E.; Nakazawa, Y.; Narymbetov, B. Z.; Kato, K.; Kobayashi, H.; Kobayashi, A.; Tokumoto, M.; Cassoux, P. *J. Am. Chem. Soc.* **2001**, *123*, 306−314.
(13) Kobayashi, H.; Tanaka, H.; Ojima, E.; Fujiwara, H.; Nakazawa, Y.; Otsuka, T.; Kobayashi, A.; Tokumoto, M.; Cassoux, P. *Synth. Met.* **2001**, *120*, 663−666.
(14) Kobayashi, H.; Tanaka, H.; Ojima, E.; Fujiwara, H.; Otsuka, T.; Kobayashi, A.; Tokumoto, M.; Cassoux, P. *Polyhedron* **2001**, *20*, 1587−1592.
(15) Tanaka, H.; Kobayashi, H.; Kobayashi, A.; Cassoux, P. *Adv. Mater.* **2000**, *12*, 1685−1689.
(16) Ojima, E.; Fujiwara, H.; Kato, K.; Kobayashi, H.; Tanaka, H.; Kobayashi, A.; Tokumoto, M.; Cassoux, P. *J. Am. Chem. Soc.* **1999**, *121*, 5581−5582.
(17) Alberola, A.; Coronado, E.; Galán-Mascarós, J. R.; Giménez-Saiz, C.; Gómez-García, C. J. *J. Am. Chem. Soc.* **2003**, *125*, 10774−10775.

(18) Coronado, E.; Galán-Mascarós, J. R.; Gómez-García, C. J. *J. Chem. Soc., Dalton Trans.* **2000**, 205−210.
(19) Coronado, E.; Galán-Mascarós, J. R.; Giménez-Saiz, C.; Gómez-García, C. J.; Martínez-Agudo, J. M.; Martínez-Ferrero, E. *Polyhedron* **2003**, *22*, 2381−2386.
(20) Coronado, E.; Curreli, S.; Giménez-Saiz, C.; Gómez-García, C. J.; Alberola, A. *Inorg. Chem.* **2006**, *45*, 10815−10824.
(21) Martin, L.; Day, P.; Barnett, S. A.; Tocher, D. A.; Horton, P. N.; Hursthouse, M. B. *CrystEngComm* **2008**, *10*, 192−196.
(22) Martin, L.; Turner, S. S.; Day, P.; Guionneau, P.; Howard, J. A. K.; Uruichi, M.; Yakushi, K. *J. Mater. Chem.* **1999**, *9*, 2731−2736.
(23) Martin, L.; Day, P.; Clegg, W.; Harrington, R. W.; Horton, P. N.; Bingham, A.; Hursthouse, M. B.; McMillan, P.; Firth, S. *J. Mater. Chem.* **2007**, *17*, 3324−3329.
(24) Martin, L.; Day, P.; Nakatsuji, S.; Yamada, J.; Akutsu, H.; Horton, P. *CrystEngComm* **2010**, *12*, 1369−1372.
(25) Zhang, B.; Zhang, Y.; Liu, F.; Guo, Y. *CrystEngComm* **2009**, *11*, 2523−2528.
(26) Martin, L.; Day, P.; Nakatsuji, S.; Yamada, J.; Akutsu, H.; Horton, P. N. *Bull. Chem. Soc. Jpn.* **2010**, *83*, 419−423.
(27) Rashid, S.; Turner, S. S.; Day, P.; Light, M. E.; Hursthouse, M. B. *Inorg. Chem.* **2000**, *39*, 2426−2428.
(28) Coronado, E.; Galán-Mascarós, J. R.; Giménez-Saiz, C.; Gómez-García, C. J.; Ruiz-Perez, C. *Eur. J. Inorg. Chem.* **2003**, 2290−2298.
(29) Coronado, E.; Galán-Mascarós, J. R.; Giménez-Saiz, C.; Gómez-García, C. J.; Ruiz-Pérez, C.; Triki, S. *Adv. Mater.* **1996**, *8*, 737−740.
(30) Alberola, A.; Coronado, E.; Galán-Mascarós, J. R.; Giménez-Saiz, C.; Gómez-García, C. J.; Romero, F. M. *Synth. Met.* **2003**, *133*, 509−513.
(31) Galán-Mascarós, J. R.; Coronado, E.; Goddard, P. A.; Singleton, J.; Coldea, A. I.; Wallis, J. D.; Coles, S. J.; Alberola, A. *J. Am. Chem. Soc.* **2010**, *132*, 9271−9273.
(32) Coronado, E.; Galán-Mascarós, J. R. *J. Mater. Chem.* **2005**, *15*, 66−74.
(33) Coronado, E.; Galán-Mascarós, J. R.; Gómez-García, C. J.; Martínez-Ferrero, E.; van Smaalen, S. *Inorg. Chem.* **2004**, *43*, 4808−4810.
(34) Klehe, A. K.; Lauhkin, V.; Goddard, P. A.; Symington, J. A.; Aghassi, J.; Singleton, J.; Coronado, E.; Galán-Mascarós, J. R.; Gómez-García, C. J.; Giménez-Saiz, C. *Synth. Met.* **2003**, *133*, 549−551.
(35) Alberola, A.; Coronado, E.; Galán-Mascarós, J. R.; Giménez-Saiz, C.; Gómez-García, C. J.; Martínez-Ferrero, E.; Murcia-Martínez, A. *Synth. Met.* **2003**, *135*, 687−689.
(36) Coronado, E.; Forment-Aliaga, A.; Galán-Mascarós, J. R.; Giménez-Saiz, C.; Gómez-García, C. J.; Martínez-Ferrero, E.; Nuez, A.; Romero, F. M. *Solid State Sci.* **2003**, *5*, 917−924.
(37) Martin, L.; S. Turner, S.; Day, P.; M. Abdul Malik, K.; J. Coles, S.; Hursthouse, M. B. *Chem. Commun.* **1999**, 513−514.
(38) Martin, L.; Turner, S. S.; Day, P. *Synth. Met.* **1999**, *102*, 1638−1641.
(39) Martin, L.; Turner, S. S.; Day, P.; Guionneau, P.; Howard, J. A. K.; Hibbs, D. E.; Light, M. E.; Hursthouse, M. B.; Uruichi, M.; Yakushi, K. *Inorg. Chem.* **2001**, *40*, 1363−1371.
(40) Akutsu-Sato, A.; Akutsu, H.; Yamada, J.; Nakatsuji, S.; Turner, S. S.; Day, P. *J. Mater. Chem.* **2007**, *17*, 2497−2499.
(41) Prokhorova, T. G.; Buravov, L. I.; Yagubskii, E. B.; Zorina, L. V.; Khasanov, S. S.; Simonov, S. V.; Shibaeva, R. P.; Korobenko, A. V.; Zverev, V. N. *CrystEngComm* **2011**, *13*, 537−545.
(42) Turner, S. S.; Day, P.; Malik, K. M. A.; Hursthouse, M. B.; Teat, S. J.; MacLean, E. J.; Martin, L.; French, S. A. *Inorg. Chem.* **1999**, *38*, 3543−3549.
(43) Rashid, S.; Turner, S. S.; Day, P.; Howard, J. A. K.; Guionneau, P.; McInnes, E. J. L.; Mabbs, F. E.; Clark, R. J. H.; Firth, S.; Biggs, T. *J. Mater. Chem.* **2001**, *11*, 2095−2101.
(44) Sun, S. Q.; Wu, P. J.; Zhang, Q. C.; Zhu, D. B. *Mol. Cryst. Liq. Cryst.* **1998**, *319*, 259−269.
(45) Sun, S.; Wu, P.; Zhang, Q.; Zhu, D. *Synth. Met.* **1998**, *94*, 161−166.
(46) Zorina, L.; Prokhorova, T.; Simonov, S.; Khasanov, S.; Shibaeva, R.; Manakov, A.; Zverev, V.; Buravov, L.; Yagubskii, E. *J. Exp. Theor. Phys.* **2008**, *106*, 347−354.
(47) Zorina, L. V.; Khasanov, S. S.; Simonov, S. V.; Shibaeva, R. P.; Zverev, V. N.; Canadell, E.; Prokhorova, T. G.; Yagubskii, E. B. *CrystEngComm* **2011**, *13*, 2430−2438.
(48) Coronado, E.; Curreli, S.; Giménez-Saiz, C.; Gómez-García, C. J. *J. Mater. Chem.* **2005**, *15*, 1429−1436.
(49) Prokhorova, T. G.; Khasanov, S. S.; Zorina, L. V.; Buravov, L. I.; Tkacheva, V. A.; Baskakov, A. A.; Morgunov, R. B.; Gener, M.; Canadell, E.; Shibaeva, R. P.; Yagubskii, E. B. *Adv. Funct. Mater.* **2003**, *13*, 403−411.
(50) Akutsu-Sato, A.; Kobayashi, A.; Mori, T.; Akutsu, H.; Yamada, J.; Nakatsuji, S.; Turner, S. S.; Day, P.; Tocher, D. A.; Light, M. E.; Hurstho, M. B. *Synth. Met.* **2005**, *152*, 373−376.
(51) Coronado, E.; Curreli, S.; Giménez-Saiz, C.; Gómez-García, C. J. *Synth. Met.* **2005**, *154*, 245−248.
(52) Akutsu, H.; Akutsu-Sato, A.; Turner, S. S.; Day, P.; Canadell, E.; Firth, S.; Clark, R. J. H.; Yamada, J.; Nakatsuji, S. *Chem. Commun.* **2004**, 18−19.
(53) Martin, L.; Day, P.; Akutsu, H.; Yamada, J.; Nakatsuji, S.; Clegg, W.; Harrington, R. W.; Horton, P. N.; Hursthouse, M. B.; McMillan, P.; Firth, S. *CrystEngComm* **2007**, *9*, 865−867.
(54) Kanehama, R.; Yoshino, Y.; Ishii, T.; Manabe, T.; Hara, H.; Miyasaka, H.; Matsuzaka, H.; Yamashita, M.; Katada, M.; Nishikawa, H.; Ikemoto, I. *Synth. Met.* **2003**, *133*, 553−554.
(55) Rashid, S.; Turner, S. S.; Le Pevelen, D.; Day, P.; Light, M. E.; Hursthouse, M. B.; Firth, S.; Clark, R. J. H. *Inorg. Chem.* **2001**, *40*, 5304−5306.
(56) Akutsu, H.; Akutsu-Sato, A.; Turner, S. S.; Le Pevelen, D.; Day, P.; Laukhin, V.; Klehe, A.; Singleton, J.; Tocher, D. A.; Probert, M. R.; Howard, J. A. K. *J. Am. Chem. Soc.* **2002**, *124*, 12430−12431.
(57) Coldea, A. I.; Bangura, A. F.; Singleton, J.; Ardavan, A.; Akutsu-Sato, A.; Akutsu, H.; Turner, S. S.; Day, P. *Phys. Rev. B* **2004**, *69*, 085112.
(58) Martin, L.; Turner, S.; Day, P.; Mabbs, F. E.; McInnes, E. J. L. *Chem. Commun.* **1997**, 1367−1368.
(59) Martin, L.; Day, P.; Horton, P.; Nakatsuji, S.; Yamada, J.; Akutsu, H. *J. Mater. Chem.* **2010**, *20*, 2738−2742.
(60) Madalan, A. M.; Canadell, E.; Auban-Senzier, P.; Branzea, D.; Avarvari, N.; Andruh, M. *New J. Chem.* **2008**, *32*, 333−339.
(61) Coronado, E.; Curreli, S.; Giménez-Saiz, C.; Gómez-García, C. J.; Deplano, P.; Mercuri, M. L.; Serpe, A.; Pilia, L.; Faulmann, C.; Canadell, E. *Inorg. Chem.* **2007**, *46*, 4446−4457.
(62) Gómez-García, C. J.; Coronado, E.; Curreli, S.; Giménez-Saiz, C.; Deplano, P.; Mercuri, M. L.; Pilia, L.; Serpe, A.; Faulmann, C.; Canadell, E. *Chem. Commun.* **2006**, 4931−4933.
(63) Clemente-Leon, M.; Coronado, E.; Gómez-García, C. J.; Soriano-Portillo, A.; Constant, S.; Frantz, R.; Lacour, J. *Inorg. Chim. Acta* **2007**, *360*, 955−960.
(64) Coronado, E.; Galán-Mascarós, J. R.; Gómez-García, C. J.; Murcia-Martínez, A.; Canadell, E. *Inorg. Chem.* **2004**, *43*, 8072−8077.
(65) Riobe, F.; Piron, F.; Rethore, C.; Madalan, A. M.; Gómez-García, C. J.; Lacour, J.; Wallis, J. D.; Avarvari, N. *New J. Chem.* **2011**, *35*, 2279−2286.
(66) Bangura, A. F.; Coldea, A. I.; Ardavan, A.; Singleton, J.; Akutsu-Sato, A.; Akatsu, H.; Day, P. *J. Phys. IV* **2004**, *114*, 285−287.
(67) Gambardella, A.; Di Capua, R.; Salluzzo, M.; Vaglio, R.; Affronte, M.; del Pennino, U.; Curreli, S.; Giménez-Saiz, C.; Gómez-García, C. J.; Coronado, E. *Solid State Sci.* **2008**, *10*, 1773−1776.
(68) Lardiés, N.; Coronado, E.; Curreli, S.; Gómez-García, C. J.; Giménez-Saiz, C. In *Proccedings of the Seventh International Symposium on Crystalline Organic Metals, Superconductors and Ferromagnets*, Peñiscola, Spain, Sept 24−29, 2007; Vol. Book of Abstracts, p 110.
(69) Palmer, W. G. In *Experimental Inorganic Chemistry*; Cambridge University Press: New York, 1954.
(70) Otwinowski, Z.; Minor, W. In *Methods in Enzymology*; Carter, C. W. J., Sweet, R. M., Eds.; Academic Press: New York, 1997; Vol. *276*, pp 307−326.

(71) Blessing, R. H. *J. Appl. Crystallogr.* **1997**, *30*, 421−426.
(72) *CRYSALISPRO*; Oxford Diffraction: Abingdon, U.K., 2004; 171.33.55.
(73) Clark, R. C.; Reid, J. S. *Acta Crystallogr., Sect. A* **1995**, *51*, 887−897.
(74) Altomare, A.; Burla, M. C.; Camalli, M.; Cascarano, G. L.; Giacovazzo, C.; Guagliardi, A.; Moliterni, A. G. G.; Polidori, G.; Spagna, R. *J. Appl. Crystallogr.* **1999**, *32*, 115−119.
(75) Farrugia, L. J. *J. Appl. Crystallogr.* **1999**, *32*, 837−838.
(76) Sheldrick, M. *SHELX97, Programs for Crystal Structure Analysis*; Bruker AXS: Madison, WI, 1997.
(77) Leung, P. C. W.; Emge, T. J.; Beno, M. A.; Wang, H. H.; Williams, J. M.; Petricek, V.; Coppens, P. *J. Am. Chem. Soc.* **1985**, *107*, 6184−6191.
(78) Bain, G. A.; Berry, J. F. *J. Chem. Educ.* **2008**, *85*, 532−536.
(79) Bondi, A. *J. Phys. Chem.* **1964**, *68*, 441−451.
(80) Mori, T. *Bull. Chem. Soc. Jpn.* **1998**, *71*, 2509−2526.
(81) Matsumiya, S.; Izuoka, A.; Sugawara, T.; Taruishi, T.; Kawada, Y. *Bull. Chem. Soc. Jpn.* **1993**, *66*, 513−522.
(82) Williams, J. M.; Ferraro, J. R.; Thorn, R. J.; Carlson, K. D.; Geiser, U.; Wang, H. H.; Kini, A. M.; Whangbo, M. H. In *Organic Superconductors (Including Fullerenes), Synthesis, Structure, Properties and Theory*; Crimes, R. N., Ed.; Prentice Hall: Englewood Cliffs, NJ, 1992.
(83) Guionneau, P.; Kepert, C. J.; Bravic, G.; Chasseau, D.; Truter, M. R.; Kurmoo, M.; Day, P. *Synth. Met.* **1997**, *86*, 1973−1974.
(84) O'Connor, C. J. *Prog. Inorg. Chem.* **1982**, *29*, 203−283.
(85) Boca, R. *Coord. Chem. Rev.* **2004**, *248*, 757−815.